Mimicking the Intramolecular Hydrogen Bond: Synthesis, Biological Evaluation, and Molecular Modeling of Benzoxazines and Quinazolines as Potential Antimalarial Agents

Sandra Gemma,[†,‡] Caterina Camodeca,[†,‡] Margherita Brindisi,[†,‡] Simone Brogi,[†,‡] Gagan Kukreja,[†,‡] Sanil Kunjir,[†,‡] Emanuele Gabellieri,[†,‡] Leonardo Lucantoni,[‡,§] Annette Habluetzel,[‡,§] Donatella Taramelli,[†,‡,∥] Nicoletta Basilico,[†,‡,⊥] Roberta Gualdani,[#] Francesco Tadini-Buoninsegni,[#] Gianluca Bartolommei,[#] Maria Rosa Moncelli,[#] Rowena E. Martin,[▽] Robert L. Summers,[▽] Stefania Lamponi,[†,‡] Luisa Savini,[†,‡] Isabella Fiorini,[†,‡] Massimo Valoti,[○] Ettore Novellino,[†,◆] Giuseppe Campiani,*,[†,‡] and Stefania Butini[†,‡]

[†]European Research Centre for Drug Discovery and Development (NatSynDrugs), University of Siena, Via Aldo Moro, 53100 Siena, Italy

[‡]CIRM Centro Interuniversitario di Ricerche sulla Malaria, Università di Torino, Torino, Italy

[§]Scuola di Scienze del Farmaco e dei Prodotti della Salute, Università di Camerino, 62032 Camerino (MC), Italy

[∥]Dipartimento di Scienze Farmacologiche e Biomolecolari, and [⊥]Dipartimento di Scienze Biomediche, Chirurgiche e Odontoiatriche, Università di Milano, Via Pascal 36, 20133 Milan, Italy

[#]Department of Chemistry "Ugo Schiff", University of Florence, 50019 Sesto Fiorentino, Italy

[▽]Research School of Biology, The Australian National University, Canberra ACT 0200, Australia

[○]Dipartimento di Neuroscienze, University of Siena, via A. Moro 2, Siena, Italy

[◆]Dipartimento di Chimica Farmaceutica e Tossicologica, University of Naples Federico II, Via D. Montesano 49, 80131 Naples, Italy

S *Supporting Information*

ABSTRACT: The intramolecular hydrogen bond formed between a protonated amine and a neighboring H-bond acceptor group in the side chain of amodiaquine and isoquine is thought to play an important role in their antimalarial activities. Here we describe isoquine-based compounds in which the intramolecular H-bond is mimicked by a methylene linker. The antimalarial activities of the resulting benzoxazines, their isosteric tetrahydroquinazoline derivatives, and febrifugine-based 1,3-quinazolin-4-ones were examined in vitro (against *Plasmodium falciparum*) and in vivo (against *Plasmodium berghei*). Compounds **6b,c** caused modest inhibition of chloroquine transport via the parasite's "chloroquine resistance transporter" (PfCRT) in a *Xenopus laevis* oocyte expression system. In silico predictions and experimental evaluation of selected drug-like properties were also performed on compounds **6b,c**. Compound **6c** emerged from this work as the most promising analogue of the series; it possessed low toxicity and good antimalarial activity when administered orally to *P. berghei*-infected mice.
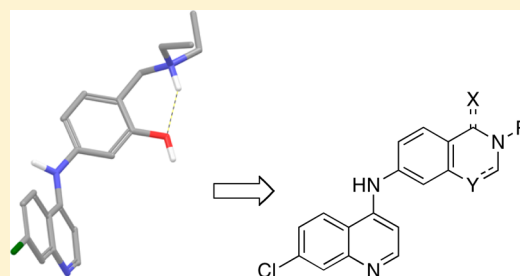
INTRODUCTION

Despite recent reductions in the malaria burden, the disease continues to impose a devastating toll upon afflicted countries in terms of morbidity, mortality, and significantly reduced economic prosperity.[1,2] The quinolines served as the mainstay for the treatment and prevention of malaria for several centuries, beginning in the seventeenth century with the use of extracts from bark of the South American Cinchona tree (which contained a number of quinolines, including quinine). Chloroquine (CQ, **1**, Chart 1) was deployed in the 1940s as a synthetic substitute for quinine, and its affordability, safety, and

efficacy made it the frontline antimalarial for more than 40 years.

However, the eventual emergence and spread of CQ-resistant (CQR) strains of the human malaria parasite, *Plasmodium falciparum*, has severely limited the usefulness of this drug and has necessitated a re-examination of chemotherapies for malaria. CQ and the related antimalarial drug amodiaquine (AQ, **2**) are both 4-aminoquinolines, yet AQ remains effective against several CQR strains of *P. falciparum*

Chart 1. Reference and Title Compounds[a]
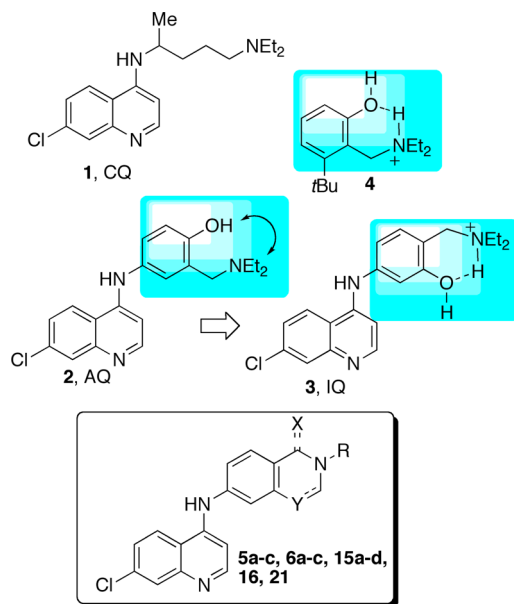
[a]Structures of title compounds **5a–c**, **6a–c**, **15a–d**, **16**, and **21** are reported in Table 1.

(Chart 1).[3–5] AQ is generally well tolerated when used as a treatment and was reintroduced in 2002 as a combination therapy with artesunate to combat multidrug resistant malaria.[6–8] Toxicity associated with the extended use of AQ is thought to be primarily due to its extensive bioactivation in vivo to form a reactive quinone-imine, which covalently binds to cell components and thereby disrupts cell function (and may also lead to antiamodiaquine immune responses).[9,10] Several studies have attempted to improve the toxicity profile of AQ,[11–14] for example, isoquine (IQ, **3**) was designed to prevent the formation of the toxic quinone-imine intermediate. Of particular note, previous work has indicated that 4-amino-quinolines carrying a single aromatic ring in the side chain are considerably more active if they contain a hydrogen bond acceptor close to a basic nitrogen.[15–19] This motif was present in early antimalarial compounds, such as **4**,[18] and is also present in AQ and IQ. Furthermore, the side chains of quinine, mefloquine, and halofantrine as well as a number of novel 4-aminoquinolines each contain a hydrogen bond acceptor group in close proximity to a protonatable amine.[15–17] The neutral form of ferroquine also contains a similar intramolecular hydrogen bond.[20] The recurrence of this intramolecular hydrogen-bonding motif, together with its importance to antimalarial activity, led us to explore the effect of mimicking it by way of a methylene linker. Using the IQ structure as a template, we introduced a methylene tether between the two heteroatoms involved in the intramolecular hydrogen bonding. In the resulting series of isoquine analogues **5a–c** (Chart 1 and Table 1), the amino and hydroxyl groups are constrained to form a benzofused oxazine ring. In addition, alkyl groups such as ethyl, n-propyl, or benzyl were placed at the benzoxazine N3 in order to explore the effect of lipophilicity and steric hindrance on antiplasmodial activity. However, the instability of the benzoxazine system under acidic hydrolytic conditions necessitated the replacement of the benzoxazine oxygen with a nitrogen atom to produce a more hydrolytically stable tetrahydroquinazoline system (**6a–c**, Chart 1 and Table 1).

Here we report the synthesis, in vitro and in vivo biological investigation, potential toxicity profiles, and molecular modeling of this novel series of 4-aminoquinolines.

■ CHEMISTRY

In general, the syntheses undertaken here used inexpensive chemicals and required relatively few steps. The synthesis of compounds **5a–c** is reported in Scheme 1. For the synthesis of **5a,b**, the key intermediates **9a,b** were prepared following a described two-step procedure.[18,21] The first step involved a Mannich reaction involving the commercially available 3-hydroxyacetanilide **7** and the suitable amine to provide the corresponding Mannich products **8a,b**. The amide function was then hydrolyzed with aqueous hydrochloric acid, and the 3-aminophenols thus obtained were coupled with 4,7-dichloroquinoline.

Reaction of **9a,b** with formaldehyde led to the closure of the benzoxazine ring, producing compounds **5a,b** in reasonable yield after chromatographic purification. The benzyl-derivative **5c** was synthesized using an alternative synthetic procedure (Scheme 1). Accordingly, intermediate **10**, prepared as previously described,[22,23] was reacted with the Schiff base formed by treatment of benzylamine with formaldehyde. The resulting Mannich product was exposed to an excess of formaldehyde leading to the ring closure.[24] Compound **5c** was precipitated from the reaction crude, and the resulting solid was then purified by crystallization.

The synthesis of **6a–c**, **15a–d**, and **16** is outlined in Scheme 2. 4-Nitroanthranilic acid **11**[25] was coupled with the suitable amines to yield intermediates **12a,b,d**.

The latter amides were then treated with formic acid to form the quinazolinone ring of **13a,b** or with trimethylorthoformate and p-toluensulfonic acid to produce **13d**. A different synthetic approach was used to prepare intermediate **13c** in one step from **11**; microwave irradiation of the anthranilic acid **11** in the presence of trimethylorthoformate, p-toluenesulfonic acid (PTSA), and benzylamine led to the formation of the quinazolinone **13c**, albeit with a moderate yield. The nitro group of **13a,b,d** was reduced by treatment with a Fe/CaCl₂ mixture to obtain compounds **14a,b,d**, whereas compound **13c** was reduced to **14c** using SnCl₂. Finally, anilines **14a–d** were coupled with 4,7-dichloroquinoline to yield compounds **15a–d**. Reduction of the quinazolinone system with LiAlH₄ or with alane generated in situ led to the tetrahydroquinazolines **6a,b** and **6c**, respectively. By contrast, reduction of ferrocenyl-derivative **6d** under a variety of reduction conditions invariably led to decomposition of the starting material. Reaction of **15c** with oxalyl chloride and NaCNBH₃ led to selective imine reduction, giving the dihydroquinazolinone system of compound **16**.

During the course of this study, the quinazolinone **21**, an analogue of **15c** bearing a protonatable side chain, was also synthesized (Scheme 3). 4-Cyanobenzaldehyde **17** was submitted to a reductive amination protocol which exploits α-picoline-borane as a less toxic alternative to NaCNBH₃.[27] Amine **19** was then obtained through reduction of the nitrile group of **18** using nickel boride generated in situ from NiCl₂ and NaBH₄.[28] Coupling of **19** with the anthranilic acid derivative **11** followed by cyclization led to the key intermediate **20**. This latter compound was then reduced, and the resulting aniline was coupled with 4,7-dichloroquinoline to afford **21**.

Table 1. Ionic Forms, in Vitro Antiplasmodial Activity, and Cytotoxicity of Title and Reference Compounds

Cpd	Structure	Calculated Ionic Forms (%)[a]		IC$_{50}$ (nM)[b]		RI[e]	TC$_{50}$ (µM)[f]	
		pH 7.4	pH 5.5	D10[c]	W2[d]		3T3	HepG2
5a		DP 0 P 7 N 93	DP 27 P 63 N 10	23	72	3.1	29	6.0
5b		DP 0 P 7 N 93	DP 27 P 63 N 10	21	40	2.0	nt	nt
5c		DP 0 P 1 N 99	DP 12 P 39 N 49	38	31	0.8	40	15
6a		DP 0 P 48 N 52	DP 18 P 81 N 1	11	60	5.4	nt	nt
6b		DP 0 P 49 N 51	DP 18 P 81 N 1	21	53	2.5	17	5.7
6c		DP 0 P 9 N 91	DP 16 P 74 N 10	53	67	1.3	40	25
15a		P 1 N 99	P 52 N 48	>1000	>1000	-	nt	nt
15b		P 1 N 99	P 52 N 48	>1000	>1000	-	nt	nt
15c		P 1 N 99	P 52 N 48	>1000	>1000	-	nt	nt
15d		nc	nc	900	>1000	-	nt	nt
16		P 2 N 98	P 61 N 39	>1000	>1000	-	nt	nt
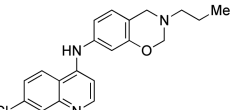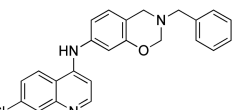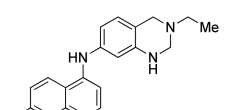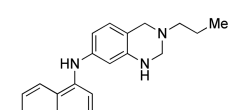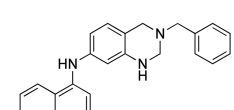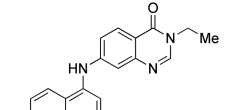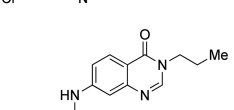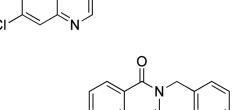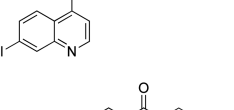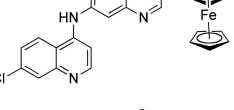
Table 1. continued

Cpd	Structure	Calculated Ionic Forms (%)[a]		IC$_{50}$ (nM)[b]		RI[e]	TC$_{50}$ (µM)[f]	
		pH 7.4	pH 5.5	D10[c]	W2[d]		3T3	HepG2
21		DP 1 P 98 N 1	DP 53 P 47 N 0	31	83	2.7	nt	nt
IQ	-	-	-	27	31	1.1	nt	nt
CQ (**1**)	-	-	-	48	681	14.2	>80	31
AQ (**2**)[e]	-	-	-	25	19	0.7	-	-

[a]Percentage of ionic form in parentheses. DP = diprotonated form; P = protonated form; N = neutral form (ACD/pK_a DB, version 11.00, software, Advanced Chemistry Development, Inc., Toronto, Canada). [b]IC$_{50}$ values are the mean of at least three determinations. Standard errors were all within 10% of the mean. [c]CQS strain. [d]CQR strain. [e]Resistance index = W2-IC$_{50}$/D10-IC$_{50}$. [f]TC$_{50}$ (toxic concentration) values are the mean of at least three determinations. Standard errors were all within 5% of the mean.

Scheme 1. Synthesis of Benzoxazine Derivatives 5a–c[a]
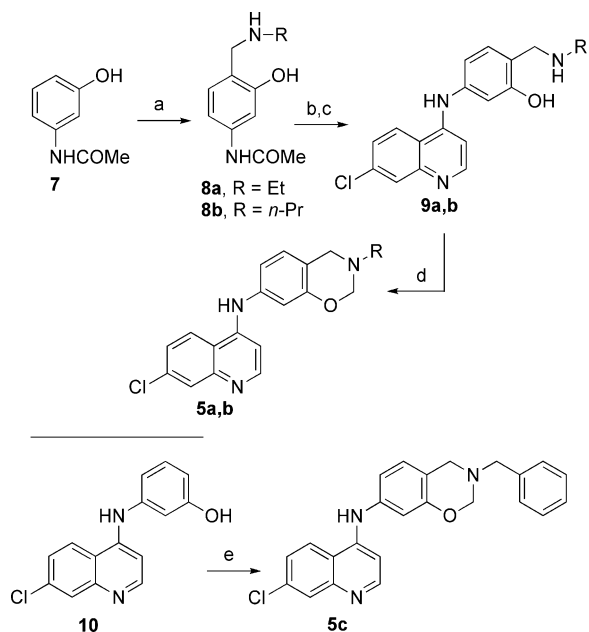
[a]Reagents and conditions: (a) RNH$_2$, HCHO 37%, EtOH, reflux, 24 h; (b) HCl 20%, EtOH, reflux, 6 h; (c) 4,7-dichloroquinoline, EtOH, reflux, 12 h; (d) KOH, HCHO 37%, MeOH, reflux,1 h; (e) HCHO 37%, benzylamine, MeOH, reflux, 3 h.

Scheme 2. Synthesis of 6a–c, 15a–d, and 16[a]
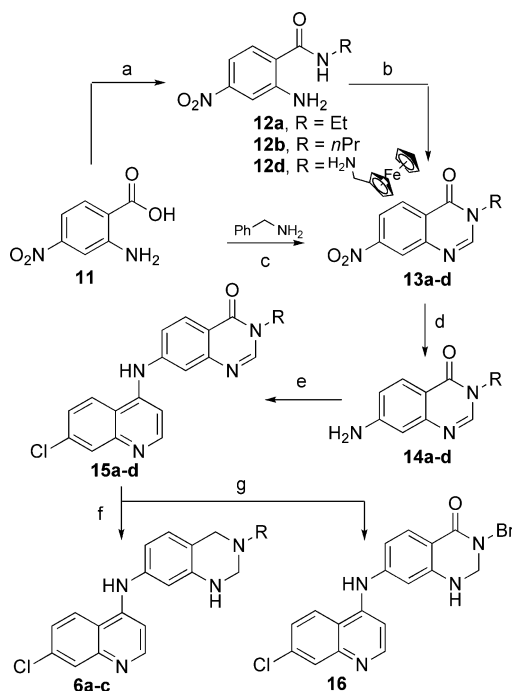
[a]Reagents and conditions: (a) EDC, HOBt, Et$_3$N, CH$_2$Cl$_2$, 0 °C, 1 h, then ethylamine (for **12a**), n-propylamine (for **12b**), or ferrocenylamine[26] (for **12d**), 25 °C, 12 h; (b) HCOOH, neat, 110 °C, 3 h (for **13a,b**) or CH(OMe)$_3$, PTSA, reflux 3 h (for **13d**); (c) CH(OMe)$_3$, benzylamine (for **13c**), PTSA, neat, MW, 150 °C, 150 W, 3 × 10 min; (d) Fe, CaCl$_2$, 75% EtOH, reflux, 2 h (for **14a,b,d**) or SnCl$_2$·2H$_2$O, AcOEt, reflux, 2 h (for **14c**); (e) 4,7-dichloroquinoline, EtOH, reflux, 18–48 h; (f) LiAlH$_4$, dry THF, reflux, 4 h (for **6a,b**) or AlH$_3$ (prepared in situ), dry THF, 25 °C, 1 h (for **6c**); (g) (i) (COCl)$_2$, CHCl$_3$, reflux, 1 h, (ii) NaCNBH$_3$, dry THF, 25 °C, 24 h.

■ RESULTS AND DISCUSSION

Antiplasmodial Activity and Structure–Activity Relationships (SARs). The antiplasmodial activities of the synthesized compounds were measured in vitro against human red blood cells infected with either the D10 (CQ-sensitive; CQS) or the W2 (CQR) strain of *P. falciparum*. The IC$_{50}$ values (presented in Table 1) were determined using a parasite lactate dehydrogenase (pLDH) assay.[29]

To verify our design approach, we performed a conformational analysis on the structure of protonated IQ, AQ, and halofantrine. As shown in Figure S1 of the Supporting Information, the analysis confirmed that the lower energy conformations of these drugs contain an intramolecular hydrogen bond between the phenolic oxygen and the ammonium nitrogen. These data indicate that the six-membered ring feature of IQ is closely mimicked by the benzoxazine ring of derivative **5a**. Benzoxazine derivatives **5a–c** showed potent antiplasmodial activity against both CQR and

Scheme 3. Synthesis of 21[a]
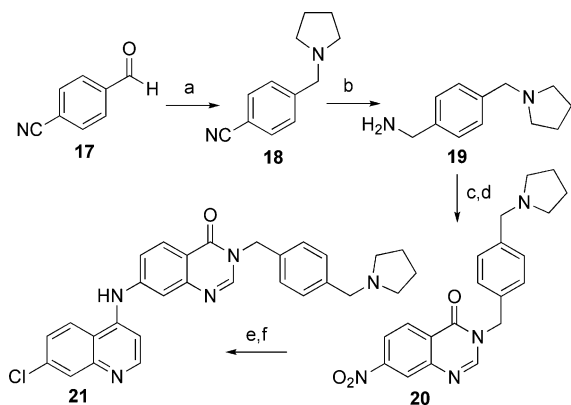
[a]Reagents and conditions: (a) pyrrolidine, AcOH, pic-BH$_3$, neat, 25 °C, 3 h; (b) NiCl$_2$·6H$_2$O, NaBH$_4$, EtOH, 25 °C, 12 h; (c) **11**, EDC, HOBt, Et$_3$N, CH$_2$Cl$_2$, 0 °C, 1 h, then **19**, 25 °C, 12 h; (d) HCOOH, neat, 110 °C, 3 h; (e) Fe, CaCl$_2$, EtOH 75%, reflux, 2 h; (f) 4,7-dichloroquinoline, pyridinium chloride, EtOH, reflux, 18 h.

CQS parasites. Indeed, the IC$_{50}$ values determined for **5a–c** in the CQS strain were comparable to those measured in these parasites for IQ, AQ, and CQ. However, only one of the compounds (**5c**) was equally active against both CQS and CQR strains, with a resistance index (RI) of 0.8 (the RI is the IC$_{50}$ value measured in the CQR strain divided by that measured in the CQS strain).

Increases in the lipophilicity of the substituents were associated with modest increases in potency against the CQR strain (**5c** > **5b** > **5a**), but this trend was not observed in the CQS strain. Likewise, the finding that the RI values calculated for compounds **5a–c** decrease with increasing lipophilicity (3.1, 2.0, and 0.8, respectively) supports the idea that activity against CQR parasites is influenced by the lipophilicity of the substituent. NMR-based stability studies revealed that compounds **5a–c** were stable in a DMSO/D$_2$O solution for several days at 25 °C. However, rapid opening of the benzoxazine ring occurred in the presence of an aqueous or methanolic solution of DCl. Furthermore, when incubated at 37 °C, compounds **5a–c** were stable at pH 7.4 but became unstable after only 1 h at pH 2. We therefore performed isosteric replacement of the benzoxazine O with a NH group in order to increase chemical stability, which yielded quinazolines **6a–c**. NMR studies confirmed that compounds **6a–c** were stable for 24 h at 37 °C under both neutral and acidic conditions. The tetrahydroquinazoline derivatives **6a,b** (which possess ethyl and *n*-propyl substituents, respectively, at the tetrahydroquinazoline N3) exhibited potent activities against the CQS strain but were less effective against CQR parasites (RI = 5.4 and 2.5, respectively). It is worth noting that the two compounds that bear a lipophilic benzyl group (**5c** and **6c**) were equally active against CQR and CQS strains (RI = 0.8 and 1.3, respectively). This suggests that they evade, or are not significantly affected by, the mechanisms underlying resistance to CQ.

The primary determinant of CQ resistance in *P. falciparum* are mutations in the "chloroquine resistance transporter" (PfCRT). The resistance-conferring form of PfCRT (PfCRT^{CQR}) mediates the efflux of CQ out of the digestive vacuole (DV), away from its site of accumulation and action, whereas the sensitive form (PfCRT^{CQS}) lacks this ability.[30,31] We investigated interactions between PfCRT and compounds

6b and **6c** using a *X. laevis* oocyte expression system.[31] The direction of PfCRT^{CQR}-mediated CQ transport in this system is from the mildly acidic extracellular medium (pH 6.0) into the oocyte cytosol (pH 7.2), which corresponds to the efflux of CQ from the acidic DV (pH ∼ 5.5) into the parasite cytosol (pH 7.3). In an initial experiment in which the derivatives were tested at an extracellular concentration of 100 μM, both **6b** and **6c** caused modest but statistically significant reductions in the uptake of CQ via PfCRT^{CQR} (Figure 1A; $P < 0.001$, ANOVA) and did not affect the passive diffusion of CQ into oocytes expressing PfCRT^{CQS} ($P > 0.05$, ANOVA). It is worth noting that in this screen, both **6b** and **6c** were considerably less potent inhibitors of PfCRT^{CQR} than the CQ resistance-reverser verapamil.

Moreover, an analysis of the concentration-dependent inhibition of PfCRT^{CQR} by **6c** (Figure 1B) yielded an IC$_{50}$ value (228 ± 25 μM; $n = 4$) that is significantly higher than that measured previously for verapamil (30 ± 1 μM[31]) or saquinavir (13 ± 0.9 μM;[32] the most potent PfCRT^{CQR} inhibitor reported to date). Taken together, the data indicate that **6b** and **6c** have relatively low affinities for PfCRT^{CQR}.

A third series of isoquine analogues (**15a–d**) bearing a N3-substituted 1,3-quinazolin-4-one scaffold (based on the potent antimalarial compound febrifugine) were synthesized and their antiplasmodial activities tested. The ferrocenylmethyl side chain of compound **15d** is more lipophilic than a benzyl group and has a peculiar electrochemical behavior, making it an attractive moiety to be exploited for the development of novel antimalarials.[33] The very high IC$_{50}$ values (>1000 nM) obtained for **15a–d** and the partially reduced intermediate **16** are likely to be due, at least in part, to poor accumulation of these compounds in the DV. For instance, compounds **15a–d** and **16** are predicted to possess only one protonatable N, moreover the calculated distribution of protonated species indicates that they are very weak bases. Hence, these quinazolinone intermediates are not expected to accumulate to high levels in the DV via the weak-base trapping mechanism.

However, the addition of another protonatable moiety to **15c** (to give compound **21**) greatly improved protonatability (53% in a diprotonated form at pH 5.5; Table 1) and restored antiplasmodial activity against CQS and CQR parasites at nanomolar concentrations.

In Silico Prediction and Experimental Evaluation of Selected Drug-Like Properties. In silico drug-likeness of compounds **5a–c** and **6a–c** was calculated using the OSIRIS molecular property explorer (Actelion Pharmaceuticals Ltd., Allschwil, Switzerland Table S1 of the Supporting Information). LogP and log S values were calculated, along with drug-likeness and drug-score parameters, for **5a–c** and **6a–c** as well as for IQ, CQ, and AQ (Table 2).

The data indicates that **5a–c** and **6a–c** are likely to be less soluble in water than the reference antimalarials. The program identified structural fragments within **5a–c** and **6c** that may increase the risk of mutagenic side effects. These molecular fragments are often observed in toxic compounds (as listed in the RTECS database) but are less frequently observed in approved drugs (the assumption being that approved drugs are devoid of major toxicity issues).

These findings led us to undertake in vitro assessments of selected drug-like and toxicity properties. Specifically, the (a) solubility and chemical stability, (b) metabolic stability, and (c) cytotoxicity and genotoxicity of the compounds were determined.
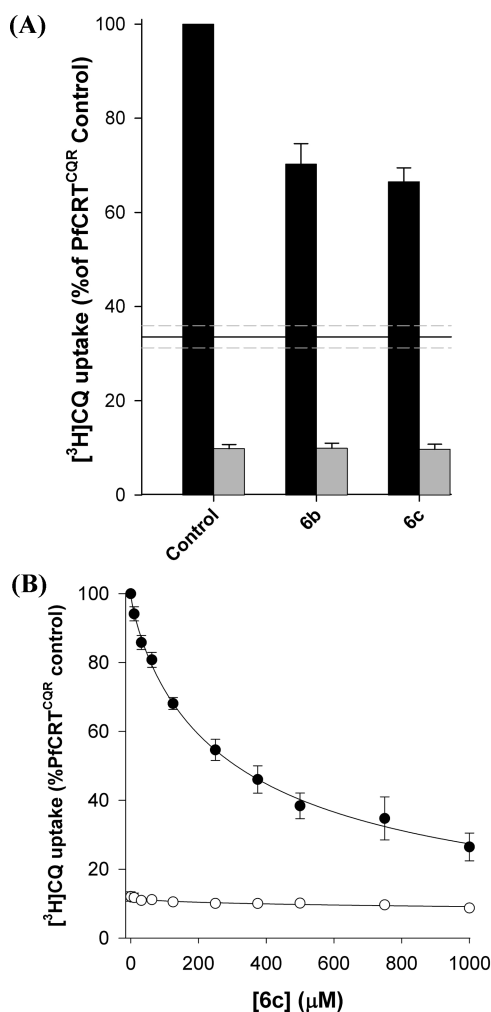
Figure 1. (A) [³H]CQ uptake into oocytes expressing Dd2 PfCRT^CQR (black bars) or D10 PfCRT^CQS (gray bars) in the presence of 100 μM of **6b** or **6c**. Both compounds caused modest but statistically significant reductions in CQ uptake via PfCRT^CQR ($P < 0.001$; ANOVA). The level of inhibition by verapamil is represented as a solid line with the SEM from $n = 4$ represented by gray dashed lines. (B) The concentration-dependent effect of **6c** on the uptake of [³H]CQ into oocytes expressing Dd2 PfCRT^CQR (closed circles) or D10 PfCRT^CQS (open circles). The IC$_{50}$ value derived from the data for **6c** (228 ± 25 μM; $n = 4$), was obtained by least-squares fit of the equation $Y = Y_{min} + [(Y_{max} - Y_{min})/(1 + ([\text{inhibitor}]/\text{IC}_{50})^C]$, where Y is PfCRT^CQR meditated CQ transport, Y_{min} and Y_{max} are the minimum and maximum values of Y, and C is a constant. PfCRT^CQR-mediated CQ transport was calculated by subtracting the uptake measured in oocytes expressing D10 PfCRT^CQS from that in oocytes expressing Dd2 PfCRT^CQR. Uptake is shown as the mean ± SEM from five (A) or four (B) separate experiments, within which measurements were made from 10 oocytes per treatment. Note that noninjected oocytes and oocytes expressing PfCRT^CQS take up [³H]CQ to similar (low) levels via simple diffusion of the neutral species; this represents the "background" level of CQ accumulation in oocytes (refer to ref 31 for full data and a detailed discussion).

a. Solubility and Chemical Stability. Compounds **6b,c** were tested for water solubility (at pH 3.0 and 7.4) and chemical stability (at pH 7.4). The results are summarized in Table 3. Both compounds were more soluble at pH 3.0 than at pH 7.4, but **6b** was the most soluble compound; the solubility of compound **6c** was below the limit of detection at pH 7.4

whereas **6b** was moderately soluble under the same conditions. Compound **6b** was also chemically stable at pH 7.4.

b. Metabolic Stability. An in silico analysis of the potential sites of CYP450-mediated metabolism (soft spots) for compounds **6b** and **6c** was performed using the P450 site of metabolism (SOM) prediction workflow[34] (implemented in Maestro suite 2011[35]) that predicts metabolism mediated by isoforms CYP3A4, CYP2C9, and CYP2D6. The results are presented in Figure S2 of the Supporting Information. The data indicates that **6b** and **6c** both contain soft spots at the quinoline and tetrahydroquinazoline rings and that the benzylic aromatic portion of **6c** contains an additional set of soft spots.

A preliminary assessment of the metabolic stability of **6b** and **6c** was obtained using a human recombinant CYP3A4 assay (Table 3). Compound **6b** was more resilient to CYP3A4-modification than was **6c**. This finding is consistent with the prediction (Figure S2 of the Supporting Information) that both compounds contain CYP3A4 soft spots and that **6c** is likely to be more susceptible to metabolism than **6b** because it contains an additional set of soft spots in its benzylic tail group.

The metabolic stability of compound **6b** was studied further by determining its in vitro intrinsic clearance (Cl$_{int}$) in the presence of liver microsomes. The clearance of **6b** was high in the presence of either mouse or rat liver microsomes (Table 3). When assessed in the presence of human liver microsomes (Figure 2), the natural logarithm of the percent of **6b** remaining in the nonmetabolized form decreased linearly over time, indicating that the CYP-mediated depletion of **6b** followed a monoexponential relationship. The calculated k (elimination rate constant) and Cl$_{int}$ values were 0.0192 min^{-1} and 48.0 (μL/min/mg), respectively.

In Vitro Toxicity Assays and Ames Test. Compounds **5a,c** and **6b,c** were tested for mammalian cytotoxicity in NIH3T3 (mouse embryonic fibroblast) and HepG2 (human hepatocellular liver carcinoma) cells. The resulting TC$_{50}$ values (reported in Table 1) indicate that all of the compounds possess low cytotoxic potential.

The mutagenic potential of compounds **5a,b** and **6b,c** was investigated in the *Salmonella typhimurium* strains TA98 and TA100 using the Ames test.[36,37] This assay examines the ability of compounds to cause DNA mutations. As shown in Figure 3 (TA100 strain) and in Figure S3 of the Supporting Information (TA98 strain), none of the compounds were mutagenic over the concentration range tested (5−2940 μM). The tests produced similar results when repeated in the presence of the S9 fraction of rat liver (to mimic metabolic activation of the compounds; Figure S4 of the Supporting Information).

In Vivo Antimalarial Activity against *P. berghei.* The potent antiplasmodial activities and favorable toxicity profiles of **5a** and **6b,c** encouraged a preliminary in vivo evaluation of these compounds in the *P. berghei* mouse model of malaria. In vivo testing was performed on groups of six BALB/c mice inoculated intraperitoneally with 10^7 *P. berghei*-infected erythrocytes according to the Peters 4-day test.[38] The antimalarial activity (ED$_{50}$, mg/kg) was determined by nonlinear regression (four-parameter logistic curve fit). Analogue **5a** was found to be active after intraperitoneal administration, but its lack of stability precluded oral administration (data not shown). Compounds **6b,c** both exhibited excellent oral in vivo activity, with compound **6b** slightly more effective than **6c** (ED$_{50}$ values of 8.7 and 15.7 mg/kg, respectively; Figure 4). This finding correlates well with the relative potencies of these two compounds in the in vitro assays

Table 2. Calculated Molecular Properties[a] of Compounds 5a–c, 6a–c, and the reference antimalarials IQ, AQ, and CQ

Predicted Properties	5a	5b	5c	6a	6b	6c	IQ	AQ	CQ
Drug-Score	0.14	0.11	0.09	0.34	0.30	0.19	0.57	0.57	0.67
Drug-Likeness	-0.19	-0.74	-0.64	4.37	3.75	3.82	4.41	4.55	7.39
clogP	4.62	5.08	5.55	4.19	4.65	5.12	4.94	4.94	4.37
Solubility (logS)	-5.14	-5.41	-6.17	-5.19	-5.46	-6.21	-4.45	-4.45	-4.06
Molecular Weight	339	353	401	338	352	400	355	355	319
Toxicity Risk									
Mutagenic	●	●	●	●	●	●	●	●	●

[a]Values were calculated using the OSIRIS property explorer (Actelion; http://www.organic-chemistry.org/prog/peo/). A Drug-Likeness value greater than 0 indicates that the molecule contains fragments that are frequently represented in commercially available drugs. The Drug-Score combines (i) drug-likeness, (ii) clogP, (iii) log S, (iv) molecular weight, and (v) toxicity risk. The following properties are typical of approved drugs that have low toxicity: clogP < 5, log S > −4, molecular weight < 450, drug likeness > 0, and a high drug score. Further details can be found at: http://www.rdchemicals.com/property-explorer-tutorial.html (access date 10/03/2012). Color code: green circles, no risk; yellow circle, medium risk; red circles, high risk.

Table 3. Solubility and the Chemical and in Vitro Metabolic Stability of Compounds 6b,c

property	6b	6c
solubility at pH 7.4 (μM)	53	nd[a]
solubility at pH 3.0 (μM)	231	122[b]
chemical stability (pH 7.4) (%)	100	nd
metabolic stability (hCYP3A4)[c] (%)	43 (high)	18 (low)
Cl_{int}[d] (μL/min/mg)		
mouse	219.0	
rat	121.0	

[a]The aqueous solubility was below the limit of quantitation. [b]Results refer to the largest UV peak. [c]Metabolic stability was calculated as the percentage of compound remaining after a 1 h incubation with recombinant hCYP3A4. [d]In vitro intrinsic clearance determined in the presence of liver microsomes.
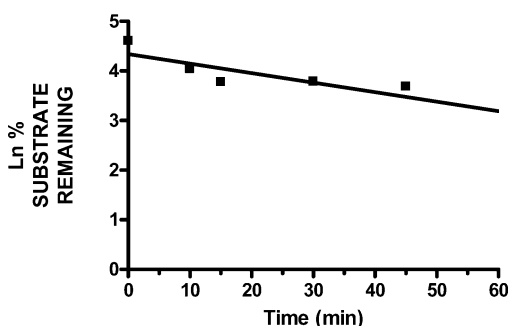

Figure 2. Time course for the depletion of **6b** in the presence of human liver microsomes. The depletion of **6b** is expressed as the natural logarithm of the percent of **6b** remaining in the non-metabolized form at each time point.

and indicates that both analogues represent lead structures for further development.

Ether-a-go-go Related Gene (hERG) K⁺ Channel and Na⁺/K⁺-ATPase Assays. To characterize the safety profile of the new antimalarials in greater detail, the effects of compounds **6b** and **6c** on the rat hERG K⁺ channel and the rabbit Na⁺/K⁺-ATPase were assessed. Both proteins are physiologically important membrane transporters that are known to be inhibited by 4-aminoquinolines (including CQ).[23,39,40]

Reducing the risk of drug-induced cardiac arrhythmia is a major hurdle in the development of new chemotherapies. The most common issue is acquired long QT syndrome, which can be caused by drugs that interfere with hERG K⁺ channels and thereby delay cardiac repolarization and increase the risk of arrhythmia. Hence, the ability to inhibit hERG K⁺ channels is considered to be an indicator of the compound's potential for producing pro-arrythmic effects. We investigated interactions between hERG K⁺ channels and compounds **6b** and **6c** using patch-clamp techniques.[41] The results are summarized in Figure 5. Compound **6b** was a potent inhibitor of the rat hERG K⁺ channel and was comparable in its inhibitory activity to the antimalarial halofantrine. By contrast, **6c** did not affect the function of the rat hERG K⁺ channel, even when tested at 10 μM.

The Na⁺/K⁺-ATPase (sodium−potassium pump) is essential to several physiological processes, including generation of the resting membrane potential and the Na⁺ gradient as well as the regulation of cell volume.[42] We tested the ability of compounds **6b** and **6c** to inhibit the hydrolytic activity of the Na⁺/K⁺-ATPase. Membrane fragments extracted from the outer medulla of rabbit kidney were treated with 10 μM of **6b**, **6c**, or ouabain (a highly specific Na⁺/K⁺-ATPase inhibitor) and the concentration of P_i measured using a colorimetric assay. As shown in Figure 6, ouabain abolished Na⁺/K⁺-ATPase activity, whereas both **6b** and **6c** only caused 35−40% reductions in hydrolytic activity. Therefore, both **6b** and **6c** have very moderate inhibitory effects on the steady-state enzyme activity and can be considered to be poor inhibitors of the Na⁺/K⁺-ATPase.

Computational Study of the hERG K⁺ Channel. The molecular basis for the different activities of **6b** and **6c** against hERG K⁺ channels were investigated by molecular docking simulation. The computational methodology employed GOLD software (The Cambridge Crystallographic Data Centre, Cambridge, UK)[43] and applied the scoring function Gold-Score[44] using a homology model of the hERG K⁺ channel[45] (available from Schrödinger;[46] see Experimental Section for further details). This computational approach was recently used
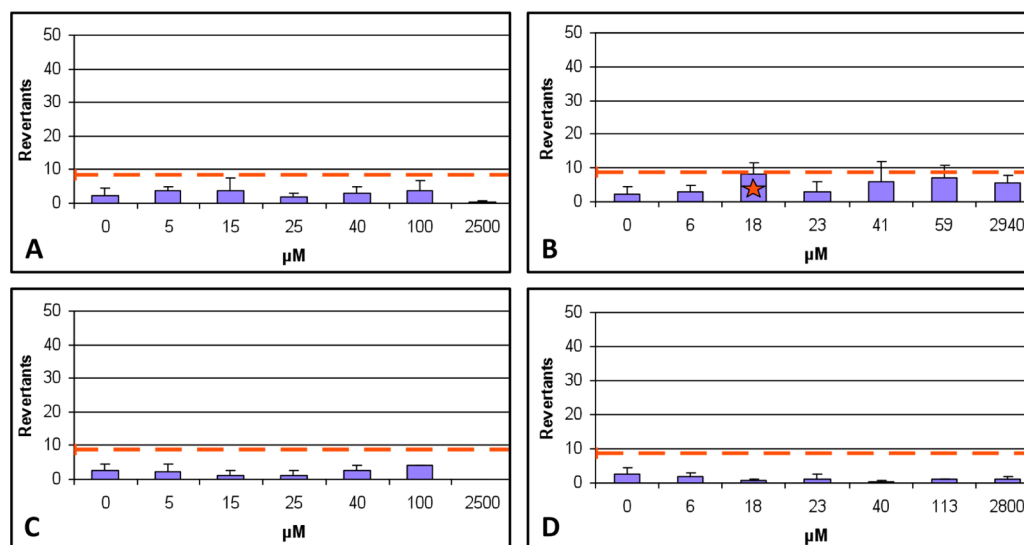
Figure 3. Ames test performed on the *S. typhimurium* TA100 strain with compound **5c** (A), **5a** (B), **6c** (C), or **6b** (D). Red star = $p < 0.01$.
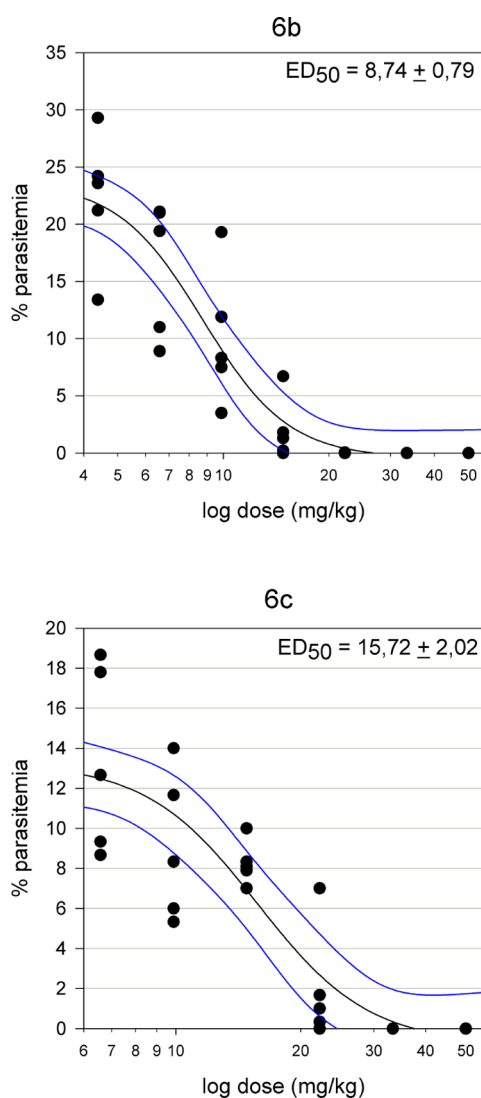

Figure 4. In vivo antimalarial activities of compounds **6b,c** in *P. berghei*-infected mice. The blue lines represent the 95% confidence limits of the fitted curve.
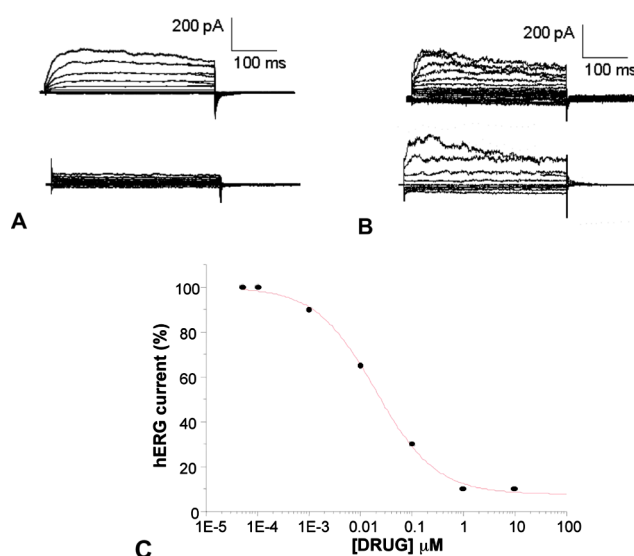

Figure 5. (A) Current traces elicited by depolarizing voltage pulse in 20 mV steps from a holding potential of −80 mV in the absence (top) or presence (bottom) of 100 nM of compound **6b**. (B) Current traces elicited by depolarizing voltage pulse in 20 mV steps from a holding potential of −80 mV in the absence (top) or presence (bottom) of 100 nM of compound **6c**. (C) Concentration-dependent blockade of the rat hERG K$^+$ channel by **6b**. The IC$_{50}$ value derived from the data is 22 ± 4 nM, and the n value (Hill coefficient) is 0.64 ± 0.07 ($n = 3$).

to explain and/or to predict the affinity of a range of compounds[47−56] (including antimalarials[57]) for hERG K$^+$ channels. The results of the docking simulation are depicted in Figure 7. The reliability of the docking results was confirmed by superimposition of docked poses of compounds **6b** and **6c** with their calculated lowest energy conformations (Figure S5 of the Supporting Information).

The two panels of Figure 7 display representative poses of the most populated cluster of docked solutions for compounds **6b** (Figure 7A) and **6c** (Figure 7B). Docking poses relative to the reference compounds CQ, AQ, IQ, and halofantrine have been also taken into consideration and are displayed in Figure S6 of the Supporting Information. The data indicates that compound **6b** strongly interacts with the key residues Y652 and
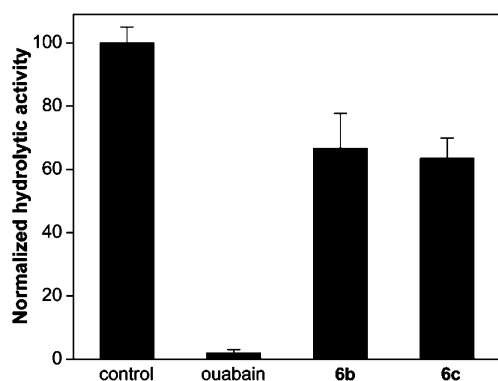
Figure 6. Hydrolytic activity of the Na$^+$/K$^+$-ATPase in the presence of 10 μM of Ouabain, **6b**, or **6c**. Values were normalized with respect to the control. The error bars represent sem ($n = 3$) or range/2 ($n = 2$).

F656 in the α and β subunits, respectively. The lowest energy arrangement (Figure 7A) allowed aromatic $\pi-\pi$ stacking interactions between these residues and the quinoline and quinazoline moieties of **6b**. Furthermore, the protonated nitrogens of compound **6b** (quinoline N1 and quinazoline N3) produced a series of H-bonds with T623α and S649γ, two of the key residues involved in hERG K$^+$ channel blockade.[49]

By contrast, the best cluster of docked positions for compound **6c** (Figure 7B and Figure S5B of the Supporting Information) suggests that it has a low-affinity interaction with the hERG K$^+$ channel. This is in part due to partial $\pi-\pi$ stacking with residues Y652 and F656 of the δ subunit because the distances between these residues and the quinoline and quinazoline moieties of **6c** exceeded 5 Å (which precludes VdW interactions and full $\pi-\pi$ stacking). Furthermore, there was no potential for interactions between the aromatic side chains of Y652γ and F656γ and the benzyl group of **6c**. In addition, for a large number of low energy poses of the most populated cluster of **6c**, polar contacts with other residues in the pocket were not evident; this may be due to steric hindrance by the benzyl group. Taken together, these observations could explain the low affinity of **6c** for the hERG K$^+$ channel. Indeed, the GoldScore value for **6c** (50.06) was similar to those calculated for CQ, IQ, and AQ (49.16, 51.93, and 51.09, respectively; these three drugs inhibit hERG in the μM range). The representative binding poses of CQ, IQ, and AQ are depicted in Figure S6 of the Supporting Information (panels A, B, and C, respectively). The interaction patterns observed for CQ, AQ, and IQ in the docking simulations, together with their respective GoldScores, were different from that observed for halofantrine, which was the most active compound analyzed (see Figure S5 of the Supporting Information). On the other hand, the GoldScore obtained for **6b** (57.42) was comparable to that of halofantrine (62.78; Figure S6D of the Supporting Information). This finding is consistent with the observation that both compounds are potent inhibitors of the hERG K$^+$ channel (**6b** IC$_{50}$ = 20 nM, halofantrine IC$_{50}$ = 40 nM[23]).

Using the best docked poses of **6b** and **6c** (Figure 7) as the starting point, 5 ns of molecular dynamics (MD) were performed with the Desmond package.[59,60] The resulting predictions were similar to those produced from the static docking calculations, as shown by superposition of the initial docked structure and the final structures (Figures S7 and S8 of the Supporting Information). The interactions depicted for compound **6b** in Figure 7 were maintained for the duration of the simulation with the exception of the H-bond with S649β.
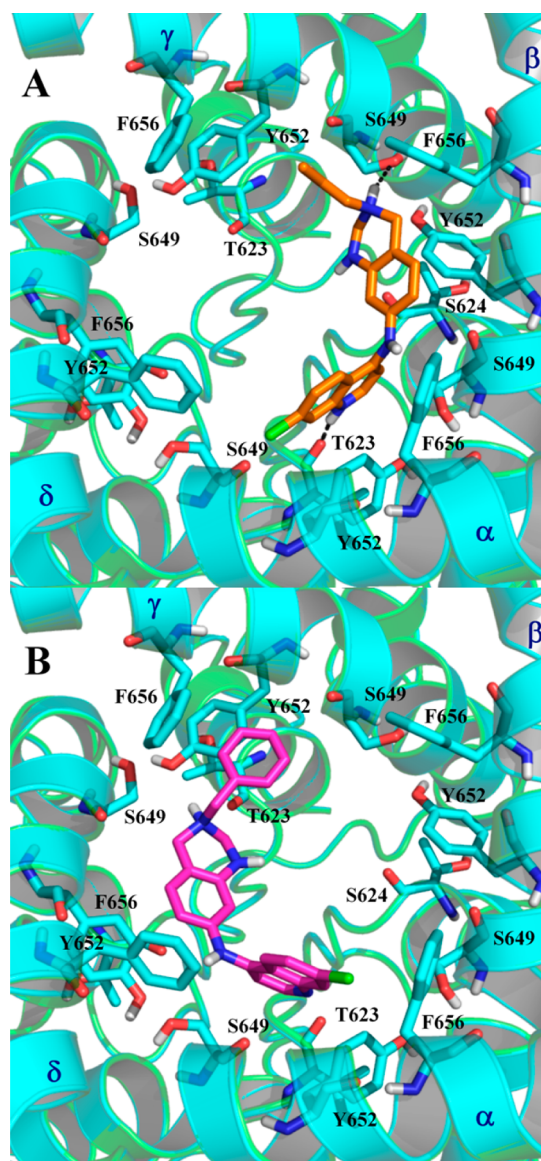

Figure 7. (A) Docked pose of **6b** (in orange sticks) in the cavity of the hERG channel (cyan cartoon; α, β, γ, and δ refers to protein subunits). It strongly interacts with residues Y652 and F656, and it forms H-bonds with key residues T623α (quinoline N1) and S649γ (N3 of the quinazoline moiety). H-bonds are represented by black dotted lines. (B) Docked pose of **6c** (in magenta sticks) in the cavity of hERG channel (cyan cartoon). It interacts weakly by partial $\pi-\pi$ stacking only with residues Y652 and F656 from δ and γ subunits. Molecular graphics were generated by PyMOL.[58] Nonpolar hydrogens were omitted for clarity.

This bond was lost in the initial steps of the simulation and was replaced by a more favorable H-bond formed between the quinazoline N3 and the backbone oxygen of residue M645β, which is known to be located in the hERG binding site (Figure S9A and Movie S1 of the Supporting Information).[52,61] Additional H-bonds were formed between the quinazoline N1 of **6b** and residues S624 (from both the β and γ subunits) and T623 (from the β subunit) (Figure S9A and Movie S1 of the Supporting Information). Moreover, as illustrated in Figures S9C and S9E of the Supporting Information, the distances monitored during MD simulation for the quinazoline and quinoline moieties remained favorable (<5 Å) for producing a strong $\pi-\pi$ stacking with Y652 from both the α

and β subunits. By contrast, the MD analysis confirmed that compound **6c** only established two (infrequent) H-bonds with the hydroxyl group of Y652γ and S649β (Figure S9B and Movie S2 of the Supporting Information) and that full $\pi-\pi$ stackings were not observed with Y652 or F656 (from γ and δ subunits, respectively) because the distance between these residues and **6c** was >5 Å (Figure S9D,F,G of the Supporting Information). These simulation results are again consistent with the observed high and low affinities, respectively, of **6b** and **6c** for the hERG channel, and as such, this work confirms that the coupling of molecular docking and MD simulations could be used to predict and/or investigate the affinity of different molecules for a given protein target.

■ CONCLUSIONS

This study describes new benzoxazine and quinazoline-based analogues of the antimalarial drugs IQ and AQ. Compounds **5a–c** possessed excellent in vitro antiplasmodial activities but were unstable in acidic conditions and were predicted to have suboptimal ADME+T properties. These issues were addressed in a series of quinazoline counterparts (compounds **6a–c**) that retained potent antiplasmodial activity, were chemically stable, and possessed significant oral in vivo activity against mouse malaria. Quinazoline **6c** emerged as the most promising analogue of this series. In addition to its potency in vivo (EC$_{50}$ of 15.7 mg/kg; oral administration), **6c** was equally active against CQS and CQR strains of *P. falciparum*. Furthermore, **6c** exhibited little or no in vitro cytotoxicity or mutagenicity and was a poor inhibitor of both the hERG K$^+$ channel and the Na$^+$,K$^+$-ATPase. However, **6b** was found to be more metabolically stable than **6c**. Computational studies provided a structural basis for the differing affinities of **6b** and **6c** for the hERG K$^+$ channel, thereby establishing a guide for the synthesis of optimized antimalarials.

■ EXPERIMENTAL SECTION

Chemistry. Starting materials and solvents were purchased from commercial suppliers and used without further purification. Reaction progress was monitored by TLC using silica gel 60 F254 (0.040−0.063 mm) with detection by UV. Silica Gel 60 (0.040−0.063 mm) or aluminum oxide 90 standardized were used for column chromatography. Yields refer to purified materials and are not optimized. ^{1}H NMR and ^{13}C NMR spectra were recorded on a Varian 300 MHz or a Bruker 400 MHz spectrometer using the residual signal of the deuterated solvent as internal standard. Splitting patterns are described as singlet (s), doublet (d), triplet (t), quartet (q), and broad (br); chemical shifts (δ) are given in ppm and coupling constants (J) in hertz (Hz). Mass spectra were recorded utilizing electrospray ionization (ESI). All moisture-sensitive reactions were performed under argon atmosphere using oven-dried glassware and anhydrous solvents. All compounds that were tested in the biological assays were analyzed by combustion analysis (CHN) to confirm the purity >95%.

N-(4-((Ethylamino)methyl)-3-hydroxyphenyl)acetamide (8a). A solution of 3-hydroxyacetanilide **7** (2.50 g, 16.5 mmol) in ethanol (15.0 mL) was added to a stirring mixture of formaldehyde (37% in water, 1.23 mL, 44.6 mmol) and ethylamine (2.0 M solution) in THF (8.3 mL, 16.6 mmol). The reaction was allowed to heat under reflux for 24 h; afterward, the solvent was removed under reduced pressure and the crude material was purified by chromatography using 5% methanol in chloroform to furnish the title compound as brown oil in 55% yield. Spectroscopic data are consistent with those reported in the literature.[21]

N-(4-((Propylamino)methyl)-3-hydroxyphenyl)acetamide (8b). Starting from **7** (2.00 g, 13.2 mmol), formaldehyde (37% in water, 0.91 mL, 33.1 mmol), and propylamine (1.1 mL, 13.2 mmol), the title

compound was obtained following the above-described procedure in 48% yield as a pale-brown oil. ^{1}H NMR (300 MHz, CDCl$_3$) δ 8.24 (br, 1H), 7.02−6.84 (m, 3H), 6.05 (br, 2H), 3.90 (s, 2H), 2.58 (t, J = 6.9 Hz, 2H), 2.00 (s, 3H), 1.54−1.46 (m, 2H), 0.89 (t, J = 7.5 Hz, 3H). MS (ESI) m/z 223 [M + H]$^+$.

N-(4-((Ethylamino)methyl)-3-hydroxyphenyl)-7-chloro-4-amino-quinoline (9a). Aqueous HCl (20% solution, 3.5 mL) was added to **8a** (0.63 g, 3.02 mmol), and the solution was heated under reflux for 6 h. The solvent was then removed in vacuo, and the resulting residue coevaporated with ethanol to give the corresponding hydrochloride salt. To a solution of the latter salt in ethanol (5.0 mL), 4,7-dichloroquinoline (0.66 g, 3.33 mmol) was added and the reaction was heated under reflux for 12 h. Thereafter, the solvent was removed under reduced pressure and the residue purified by silica gel flash column chromatography (5% methanol in chloroform) to yield the quinoline hydrochloride salt. To obtain the compound as a free base, the solid was dissolved in water and a saturated solution of NaHCO$_3$ was added. The aqueous solution was extracted with dichloromethane and dried over Na$_2$SO$_4$, and the solvent was removed in vacuo to afford the desired product in 78% yield as a pale-brown solid. Spectroscopic data are consistent with those reported in the literature.[21]

N-(4-((Propylamino)methyl)-3-hydroxyphenyl)-7-chloro-4-ami-noquinoline (9b). Starting from **8b** (0.59 g, 2.66 mmol), the title compound was obtained following the above-described procedure in 74% yield as a pale-brown solid. ^{1}H NMR (300 MHz, CDCl$_3$) δ 8.44 (m, 2H), 7.92 (s, 1H), 7.64 (d, J = 9.3 Hz, 1H), 7.46 (d, J = 7.8 Hz, 1H), 7.04 (m, 3H), 4.23 (s, 2H), 4.03 (s, 1H), 3.03 (t, J = 7.5 Hz, 2H), 2.63 (s, 1H), 1.77 (m, 2H), 1.04 (t, J = 7.2 Hz, 3H). MS (ESI) m/z 342 [M + H]$^+$.

N-(3-Ethyl-3,4-dihydro-2H-benzo[e][1,3]oxazin-7-yl)-7-chloro-4-aminoquinoline (5a). To a mixture of **9a** (78.0 mg, 0.24 mmol) and KOH (17.0 mg, 0.31 mmol) in methanol (2.0 mL), formaldehyde (37% in water, 58 μL, 0.78 mmol) was added. The reaction was heated under reflux for 1 h; afterward, the solvent was evaporated and the resulting residue dissolved in water. The aqueous layer was extracted with chloroform, the combined organic layers were dried over Na$_2$SO$_4$, and the solvent was removed in vacuo. The crude was purified by silica gel flash chromatography (5% methanol in chloroform) affording **5a** in 36% yield as a pale-yellow low melting solid. ^{1}H NMR (300 MHz, CDCl$_3$) δ 8.55 (d, J = 5.3 Hz, 1H), 8.03 (d, J = 2.1 Hz, 1H), 7.84 (d, J = 9.0 Hz, 1H), 7.45 (dd, J = 9.0, 2.1 Hz, 1H), 7.04−6.97 (m, 2H), 6.79 (dd, J = 8.0, 2.3 Hz, 1H), 6.72 (d, J = 2.3 Hz, 1H), 6.53 (br, 1H), 4.91 (s, 2H), 4.02 (s, 2H), 2.84 (q, J = 7.2 Hz, 2H), 1.20 (t, J = 7.2 Hz, 3H). MS (ESI) m/z 340 [M + H]$^+$. HRMS (ESI) calcd for C$_{19}$H$_{19}$ClN$_3$O [M + H]$^+$ 340.1211, found 340.1215.

N-(3-Propyl-3,4-dihydro-2H-benzo[e][1,3]oxazin-7-yl)-7-chloro-4-aminoquinoline (5b). Starting from **9b** (71 mg, 0.21 mmol), the title compound was obtained following the above-described procedure in 32% yield as a pale-yellow low melting solid. ^{1}H NMR (300 MHz, CDCl$_3$) δ 8.56 (d, J = 5.4 Hz, 1H), 8.03 (s, 1H), 7.84 (d, J = 8.9 Hz, 1H), 7.45 (dd, J = 8.9, 2.2 Hz, 1H), 7.01 (d, J = 5.4 Hz, 1H), 6.99 (d, J = 8.1 Hz, 1H), 6.79 (dd, J = 8.1, 2.2 Hz, 1H), 6.72 (s, 1H), 6.50 (s, 1H), 4.90 (s, 2H), 4.01 (s, 2H), 2.74 (t, J = 7.8 Hz, 2H), 1.57 (m, 2H), 0.96 (t, J = 7.5 Hz, 3H). ^{13}C NMR (75 MHz, CDCl$_3$) δ 155.5, 152.2, 150.0, 147.6, 139.0, 135.4, 129.3, 128.8, 126.3, 121.3, 118.3, 117.3, 115.1, 110.5, 103.0, 83.0, 53.6, 50.2, 21.5, 11.9. MS (ESI) m/z 354 [M + H]$^+$. HRMS (ESI) calcd for C$_{20}$H$_{21}$ClN$_3$O [M + H]$^+$ 354.1373, found 354.1368.

N-(3-Benzyl-3,4-dihydro-2H-benzo[e][1,3]oxazin-7-yl)-7-chloro-4-aminoquinoline (5c). To a solution of formaldehyde (37% in water, 120 μL, 0.81 mmol) in methanol (3 mL), benzylamine (80 μL, 0.81 mmol) was added and the mixture was heated under reflux for 3 h to allow the formation of the Schiff base. Successively a solution of **10**[22,23] (200 mg, 0.73 mmol) in methanol was added and the reaction was heated at 65 °C for 3 h. Thereafter, the mixture was cooled at 25 °C, and the resulting precipitate was washed with methanol, affording **5c** in 79% yield, as a pale-yellow low melting solid. ^{1}H NMR (300 MHz, CD$_3$OD) δ 8.57 (d, J = 5.3 Hz, 1H), 8.03 (d, J = 2.1 Hz, 1H), 7.86 (d, J = 9.0 Hz, 1H), 7.45 (dd, J = 9.0, 2.1 Hz, 1H), 7.30−7.38 (m, 5H),

7.04 (d, J = 5.3 Hz, 1H), 6.97 (d, J = 7.8 Hz, 1H), 6.77−6.83 (m, 2H), 6.61 (br, 1H), 4.92 (s, 2H), 3.99 (s, 2H), 3.96 (s, 2H). MS (ESI) m/z 402 [M + H]$^+$. HRMS (ESI) calcd for $C_{24}H_{21}ClN_3O$ [M + H]$^+$ 402.1373, found 402.1371.

N-Ethyl-2-amino-4-nitrobenzamide (12a). To a suspension of **11** (2.0 g, 11.0 mmol) in dry dichloromethane cooled at 0 °C, EDC (2.3 g, 12.1 mmol), HOBt (1.6 g, 12.1 mmol), and Et$_3$N (1.7 mL, 12.1 mmol) were added and the mixture was stirred at 0 °C for 1 h. Successively ethylamine (2 M in THF, 5.5 mL, 11.0 mmol) was added and the reaction was stirred at 25 °C for 12 h. Thereafter, the organic mixture was washed with saturated aqueous NaHCO$_3$, dried over Na$_2$SO$_4$, and evaporated to dryness. The residue was purified by silica gel chromatography (5% methanol in chloroform) to afford the title compound in 80% yield as yellow solid; mp (ethyl acetate/*n*-hexane) 130−132 °C. ^{1}H NMR (300 MHz, CDCl$_3$) δ 7.49 (s, 1H), 7.42 (s, 2H), 6.07 (br, 1H), 5.80 (br, 2H), 3.53−3.41 (m, 2H), 1.27 (t, J = 7.5 Hz, 3H). MS (ESI) m/z 210 [M + H]$^+$.

N-Propyl-2-amino-4-nitrobenzamide (12b). Starting from **11** (2.0 g, 11.0 mmol) and *n*-propylamine (900 µL, 11.0 mmol), the title compound was obtained following the procedure reported for **12a** in 91% yield as a yellow solid; mp (ethyl acetate/*n*-hexane) 128−130 °C. ^{1}H NMR (300 MHz, CDCl$_3$) δ 7.51 (s, 1H), 7.43 (s, 2H), 6.07 (br, 1H), 3.48−3.33 (m, 2H), 1.73−1.57 (m, 2H), 1.00 (t, J = 7.4 Hz, 3H). MS (ESI) m/z 222 [M − H]$^-$.

N-(Ferrocenylmethyl)-2-amino-4-nitrobenzamide (12d). Starting from **11** (1.1 g, 6.04 mmol) and ferrocenylamine (1.3 g, 6.04 mmol), the title compound was obtained following the above-described procedure in 89% yield as a red low melting solid. ^{1}H NMR (300 MHz, CDCl$_3$) δ 7.51 (s, 1H), 7.42 (s, 2H), 6.24 (s, 1H), 5.83 (s, 2H), 4.31 (d, J = 5.2 Hz, 2H), 4.29−4.22 (m, 2H), 4.22−4.14 (m, 7H). MS (ESI) m/z 378 [M − H]$^-$.

3-Ethyl-7-nitroquinazolin-4(3H)-one (13a). A mixture of **12a** (1.13 g, 5.4 mmol) and formic acid (2.2 mL, 57 mmol) was heated under reflux for 3 h. After cooling to 25 °C, the mixture was poured into water, and the solution was alkalinized with NaOH and extracted with chloroform. The organic phase was dried over Na$_2$SO$_4$ and evaporated under reduced pressure to afford pure **13a** in quantitative yield as a light-yellow solid; mp (ethyl acetate/*n*-hexane) 148−150 °C. ^{1}H NMR (300 MHz, CDCl$_3$) δ 8.54 (d, J = 2.2 Hz, 1H), 8.47 (d, J = 8.8 Hz, 1H), 8.25 (dd, J = 8.8, 2.2 Hz, 1H), 8.16 (s, 1H), 4.10 (q, J = 7.2 Hz, 2H), 1.45 (t, J = 7.2 Hz, 3H). MS (ESI) m/z 220 [M + H]$^+$.

7-Nitro-3-propylquinazolin-4(3H)-one (13b). Starting from **12b** (1.33 g, 6.0 mmol) and formic acid (2.4 mL, 62 mmol), the title compound was obtained following the procedure reported for **13a** in quantitative yield as a light-yellow solid; mp (ethyl acetate/*n*-hexane) 122−124 °C. ^{1}H NMR (300 MHz, CDCl$_3$) δ 8.55 (d, J = 2.2 Hz, 1H), 8.47 (d, J = 8.8 Hz, 1H), 8.26 (dd, J = 8.8, 2.2 Hz, 1H), 8.13 (s, 1H), 4.04−3.96 (m, 2H), 1.94−1.77 (m, 2H), 1.02 (t, J = 7.4 Hz, 3H). MS (ESI) m/z 234 [M + H]$^+$.

3-Benzyl-7-nitroquinazolin-4(3H)-one (13c). A mixture of 4-nitroanthranilic acid **11** (1.1 g, 6.04 mmol), trimethyl orthoformate (792 µL, 7.25 mmol), benzylamine (790 µL, 7.25 mmol), and PTSA (57 mg, 0.3 mmol) was heated by MW irradiation: 150 °C, 150 W, 3 × 10 min. Thereafter water was added, followed by alkalinization with NaOH and extraction with ethyl acetate. The organic layer was dried over Na$_2$SO$_4$, and the solvent was evaporated under reduced pressure. The crude was purified by silica gel chromatography (25% ethyl acetate in *n*-hexane) to afford the title compound in 53% yield as a pale-yellow solid; mp (methanol) 163−164 °C. ^{1}H NMR (300 MHz, CDCl$_3$) δ 8.55 (d, J = 2.2 Hz, 1H), 8.49 (d, J = 8.8 Hz, 1H), 8.27 (dd, J = 8.8, 2.2 Hz, 1H), 8.21 (s, 1H), 7.37 (s, 5H), 5.22 (s, 2H). ^{13}C NMR (75 MHz, CDCl$_3$) δ 160.1, 151.7, 148.8, 148.4, 135.2, 129.4 (2C), 129.1, 128.9, 128.4 (2C), 126.5, 123.4, 121.2, 50.2.

3-Ferrocenylmethyl-7-nitro-quinazolin-4(3H)-one (13d). A mixture of **12d** (515 mg, 1.36 mmol), trimethyl orthoformate (178 µL, 1.63 mmol), and PTSA (13 mg, 0.07 mmol) was heated under reflux for 3 h. Thereafter water was added followed by extraction with dichloromethane. The organic layer was dried over Na$_2$SO$_4$ and evaporated under reduced pressure, and the crude was purified by silica gel flash chromatography (25% ethyl acetate in *n*-hexane) to

afford **13d** in 84% yield as a reddish amorphous solid. ^{1}H NMR (300 MHz, CDCl$_3$) δ 8.51 (d, J = 2.2 Hz, 1H), 8.47 (d, J = 8.8 Hz, 1H), 8.24 (dd, J = 8.8, 2.2 Hz, 1H), 8.16 (s, 1H), 4.98 (s, 2H), 4.43−4.31 (m, 2H), 4.30−4.11 (m, 7H). MS (ESI) m/z 388 [M − H]$^-$.

7-Amino-3-ethylquinazolin-4(3H)-one (14a). To a solution of **13a** (1.05 g, 4.8 mmol) in 75% aqueous ethanol (25 mL), iron (1.74 g, 31.2 mmol) and CaCl$_2$ (705 mg, 4.8 mmol) were added and the reaction mixture was heated under reflux for 2 h. After cooling to 25 °C, the mixture was filtered through a pad of Celite and the solvent was evaporated. The resulting residue was partitioned between water and ethyl acetate. The organic extracts were dried over Na$_2$SO$_4$ and evaporated under reduced pressure, affording pure title compound as a pale-yellow solid in quantitative yield; mp (ethyl acetate/*n*-hexane) 174−176 °C. ^{1}H NMR (300 MHz, CDCl$_3$) δ 8.09 (d, J = 8.0 Hz, 1H), 7.96 (s, 1H), 6.82−6.74 (m, 2H), 4.16 (br, 2H), 4.01 (q, J = 7.2 Hz, 2H), 1.39 (t, J = 7.2 Hz, 3H). MS (ESI) m/z 190 [M + H]$^+$, 212 [M + Na]$^+$.

7-Amino-3-propylquinazolin-4(3H)-one (14b). Starting from **13b** (1.23 g, 5.4 mmol), the title compound was obtained following the procedure reported for **14a** in 96% yield as a pale-yellow solid; mp (ethyl acetate/*n*-hexane) 146−148 °C. ^{1}H NMR (300 MHz, CDCl$_3$) δ 8.04 (d, J = 8.0 Hz, 1H), 7.89 (s, 1H), 6.80−6.72 (m, 2H), 4.37 (br, 2H), 4.02−3.70 (m, 2H), 1.92−1.59 (m, 2H), 0.94 (t, J = 7.4 Hz, 3H). MS (ESI) m/z 226 [M + Na]$^+$.

7-Amino-3-benzylquinazolin-4(3H)-one (14c). To a solution of **13c** (310 mg, 1.10 mmol)) in ethyl acetate (8.0 mL), SnCl$_2$·2H$_2$O (1.37 g, 6.1 mmol) was added. The mixture was heated under reflux for 2 h and then poured into saturated aqueous NaHCO$_3$. The resulting gelatinous emulsion was filtered through a pad of Celite, and the biphasic filtrate was extracted with ethyl acetate. The combined organic extracts were dried over Na$_2$SO$_4$ and concentrated in vacuo, and the residue was purified by silica gel flash chromatography (2% methanol in dichloromethane), affording **14c** in 74% yield as a pale-yellow solid; mp (ethyl acetate/*n*-hexane) 165−168 °C. ^{1}H NMR (300 MHz, CDCl$_3$) δ 8.11 (d, J = 7.6 Hz, 1H), 8.00 (s, 1H), 7.41−7.28 (m, 5H), 6.82−6.73 (m, 2H), 5.15 (s, 2H), 4.22 (br, 2H). ^{13}C NMR (75 MHz, CDCl$_3$) δ 160.9, 152.3, 150.2, 147.2, 143.7, 136.3, 129.2, 128.9, 128.4, 128.2, 116.1, 109.2, 49.5. MS (ESI) m/z 252 [M + H]$^+$, 274 [M + Na]$^+$.

7-Amino-3-(ferrocenylmethyl)quinazolin-4(3H)-one (14d). Starting from **13d** (350 mg, 0.88 mmol), the title compound was obtained following the procedure reported for **14a** as yellow−orange solid in 91% yield; mp (ethyl acetate/*n*-hexane) 190 °C (dec.). ^{1}H NMR (300 MHz, CDCl$_3$) δ 8.09 (d, J = 9.2 Hz, 1H), 7.97 (s, 1H), 6.86−6.69 (m, 2H), 4.89 (s, 2H), 4.40−4.29 (m, 2H), 4.27−4.08 (m, 7H). MS (ESI) m/z 360 [M + H]$^+$, 382 [M + Na]$^+$.

7-((7-Chloroquinolin-4-yl)amino)-3-ethylquinazolin-4(3H)-one (15a). To a solution of **14a** (400 mg, 2.12 mmol) in ethanol (10.0 mL), 4,7-dichloroquinoline (419 mg, 2.12 mmol) was added and the reaction mixture was heated under reflux for 48 h. The resulting precipitate was collected, washed with ethanol, and dried to give the title compound in quantitative yield as a yellow solid; mp (methanol) > 300 °C. ^{1}H NMR (300 MHz, DMSO-d_6) δ 11.30 (s, 1H), 8.88 (d, J = 9.1 Hz, 1H), 8.64 (d, J = 6.9 Hz, 1H), 8.48 (s, 1H), 8.27 (d, J = 8.6 Hz, 1H), 8.18 (d, J = 2.0 Hz, 1H), 7.91 (dd, J = 9.1, 1.9 Hz, 1H), 7.76 (d, J = 1.9 Hz, 1H), 7.65 (dd, J = 8.6, 2.0 Hz, 1H), 7.13 (d, J = 6.9 Hz, 1H), 4.03 (q, J = 7.1 Hz, 2H), 1.29 (t, J = 7.1 Hz, 3H). ^{13}C NMR (75 MHz, DMSO-d_6) δ 160.1, 154.6, 150.0, 149.7, 145.0, 143.4, 140.3, 139.1, 128.7, 128.3, 126.9, 123.8, 122.1, 120.4, 117.4, 102.2, 42.0, 15.2. MS (ESI) m/z 351 [M + H]$^+$.

7-((7-Chloroquinolin-4-yl)amino)-3-propylquinazolin-4(3H)-one (15b). Starting from **14b** (400 mg, 1.97 mmol) and 4,7-dichloroquinoline (390 mg, 1.97 mmol), the title compound was obtained following the procedure described for **15a** as a yellow solid in quantitative yield; mp (methanol) > 300 °C. ^{1}H NMR (300 MHz, CD$_3$OD) δ 8.62 (d, J = 9.1 Hz, 1H), 8.50 (d, J = 7.0 Hz, 1H), 8.44−8.38 (m, 2H), 8.01 (d, J = 2.1 Hz, 1H), 7.85 (dd, J = 9.1, 2.1 Hz, 1H), 7.79 (d, J = 2.1 Hz, 1H), 7.68 (dd, J = 8.6, 2.1 Hz, 1H), 7.21 (d, J = 7.0 Hz, 1H), 4.17−3.97 (m, 2H), 1.96−1.73 (m, 2H), 1.01 (t, J = 7.4 Hz, 3H). MS (ESI) m/z 365 [M + H]$^+$.

3-Benzyl-7-((7-chloroquinolin-4-yl)amino)quinazolin-4(3H)-one (15c). Starting from **14c** (60 mg, 0.24 mmol) and 4,7-dichloroquinoline (47 mg, 0.24 mmol), the title compound was obtained following the procedure described for **15a** as a yellow solid in quantitative yield; mp (methanol) >300 °C. ^{1}H NMR (300 MHz, DMSO-d_6) δ 11.38 (br, 1H), 8.90 (d, J = 9.1 Hz, 1H), 8.64−8.60 (m, 2H), 8.26 (d, J = 8.5 Hz, 1H), 8.19 (s, 1H), 7.88 (d, J = 9.1 Hz, 1H), 7.78 (s, 1H), 7.66 (d, J = 8.5 Hz, 1H), 7.38−7.28 (m, 5H), 7.13 (d, J = 7.0 Hz, 1H), 5.23 (s, 2H). ^{13}C NMR (75 MHz, DMSO-d_6) δ 160.2, 154.8, 149.9, 149.7, 144.7, 143.6, 140.0, 139.2, 137.5, 129.3, 128.8, 128.4, 128.3, 127.1, 124.1, 122.3, 120.5, 120.1, 117.3, 102.2, 49.6. MS (ESI) m/z 413 [M + H]$^+$.

7-((7-Chloroquinolin-4-yl)amino)-3-ferrocenylquinazolin-4(3H)-one (15d). A solution of **14d** (65 mg, 0.18 mmol) and 4,7-dichloroquinoline (36 mg, 0.18 mmol) in ethanol (3.0 mL), was refluxed for 18 h. After cooling to 25 °C, the solvent was removed in vacuo and the crude purified by silica gel flash chromatography (5% methanol in chloroform), affording **15d** as a yellow amorphous solid in 50% yield. ^{1}H NMR (300 MHz, CDCl$_3$) δ 8.69 (d, J = 5.2 Hz, 1H), 8.29 (d, J = 8.7 Hz, 1H), 8.08 (d, J = 2.1 Hz, 1H), 8.05 (s, 1H), 7.92 (d, J = 9.0 Hz, 1H), 7.48 (dd, J = 9.0, 2.1 Hz, 1H), 7.45 (d, J = 2.2 Hz, 1H), 7.38−7.27 (m, 2H), 6.93 (br, 1H), 4.94 (s, 2H), 4.47−4.30 (m, 2H), 4.30−4.15 (m, 7H). MS (ESI) m/z 521 [M + H]$^+$.

N-(3-Ethyl-1,2,3,4-tetrahydroquinazolin-7-yl)-7-chloro-4-aminoquinoline (6a). To a suspension of LiAlH$_4$ (108 mg, 2.86 mmol) in dry THF (3.0 mL), a solution of **15a** (250 mg, 0.71 mmol) in THF (5.0 mL) was added dropwise and the reaction was heated under reflux for 4 h. The cooled solution was diluted with diethyl ether and washed with brine, and the organic phase was dried over Na$_2$SO$_4$ and concentrated under reduced pressure. The crude was purified by silica gel flash chromatography (5% methanol in chloroform) affording **6a** in 70% yield; mp (ethyl acetate/n-hexane) 177−179 °C. ^{1}H NMR (300 MHz, DMSO-d_6) δ 8.86 (s, 1H), 8.41−8.38 (m, 2H), 7.84 (d, J = 2.2 Hz, 1H), 7.51 (dd, J = 9.0, 2.2 Hz, 1H), 6.88−6.82 (m, 2H), 6.50−6.45 (m, 2H), 6.00 (s, 1H), 3.92 (s, 2H), 3.70 (s, 2H), 2.57−2.42 (m, 2H), 1.07 (t, J = 7.2 Hz, 3H). ^{13}C NMR (75 MHz, DMSO-d_6) δ 152.3, 149.7, 149.4, 144.8, 138.9, 134.8, 128.7, 127.7, 125.6, 125.0, 118.6, 116.0, 112.2, 108.8, 102.3, 62.3, 53.0, 46.8, 13.1. MS (ESI) m/z 339 [M + H]$^+$.

N-(3-Propyl-1,2,3,4-tetrahydroquinazolin-7-yl)-7-chloro-4-aminoquinoline (6b). Starting from **15b** (250 mg, 0.68 mmol), the title compound was prepared following the procedure reported for **6a** in 50% yield as a pale-yellow solid; mp (ethyl acetate/n-hexane) 182−184 °C. ^{1}H NMR (300 MHz, CDCl$_3$) δ 8.52 (d, J = 5.3 Hz, 1H), 8.01 (d, J = 2.0 Hz, 1H), 7.82 (d, J = 9.0 Hz, 1H), 7.43 (dd, J = 9.0, 2.0 Hz, 1H), 7.06−6.83 (m, 2H) 6.60 (dd, J = 8.0, 2.0 Hz, 1H), 6.48 (s, 2H), 4.08 (s, 2H), 3.84 (s, 2H), 2.64−2.43 (m, 2H), 1.74−1.47 (m, 2H), 0.97 (t, J = 7.4 Hz, 3H). MS (ESI) m/z 353 [M + H]$^+$. HRMS (ESI) calcd for C$_{20}$H$_{22}$ClN$_4$ [M + H]$^+$ 353.1533, found 353.1411.

N-(3-Benzyl-1,2,3,4-tetrahydroquinazolin-7-yl)-7-chloro-4-aminoquinoline (6c). To a suspension of LiAlH$_4$ (110 mg, 2.91 mmol) in dry THF (3.0 mL) cooled at 0 °C, AlCl$_3$ (130 mg, 0.97 mmol) in dry THF (2.0 mL) was added dropwise. The mixture was stirred at 0 °C for 1 h, and then a solution of **15c** (200 mg, 0.48 mmol) in dry THF (3.0 mL) was added and the reaction was stirred at 25 °C for 1 h. After cooling at 0 °C, the reaction mixture was diluted with ethyl acetate and quenched with water. The aqueous layer was extracted with ethyl acetate, the organic phase was dried over Na$_2$SO$_4$ and evaporated in vacuo. The crude was purified by silica gel flash chromatography (50% ethyl acetate in n-hexane) to afford **6c** as a pale-yellow solid in 20% yield; mp (ethyl acetate/n-hexane) 165−166 °C. ^{1}H NMR (300 MHz, CDCl$_3$) δ 8.50 (d, J = 5.3 Hz, 1H), 7.99 (d, J = 2.1 Hz, 1H), 7.84 (d, J = 9.0 Hz, 1H), 7.47−7.28 (m, 6H), 6.95 (d, J = 5.3 Hz, 1H), 6.90 (d, J = 8.0 Hz, 1H), 6.77 (br, 1H), 6.59 (d, J = 8.0, 1H), 6.48 (s, 1H), 4.08 (s, 2H), 3.86 (s, 2H), 3.76 (s, 2H). ^{13}C NMR (75 MHz, CD$_3$OD) δ 151.1, 150.4, 149.0, 144.4, 139.0, 137.6, 135.5, 129.5, 128.3, 127.4, 126.5, 125.3, 123.5, 118.3, 116.0, 113.1, 109.5, 101.6, 62.2, 57.0, 53.0. MS (ESI) m/z 401 [M + H]$^+$. HRMS (ESI) calcd for C$_{24}$H$_{22}$ClN$_4$ [M + H]$^+$ 401.1533, found 401.1553.

3-Benzyl-7-((7-chloroquinolin-4-yl)amino)-2,3-dihydroquinazolin-4(1H)-one (16). To a suspension of **15c** (100 mg, 0.24 mmol) in chloroform, oxalyl chloride (63 μL, 0.73 mmol) was added dropwise at 0 °C. After refluxing for 1 h, the solvent was evaporated and the residue dissolved in dry THF, and NaCNBH$_3$ (76 mg, 1.21 mmol) was added at 0 °C. The reaction mixture was stirred at 25 °C for 24 h, then cooled at 0 °C and treated with 5 N NaOH. The aqueous layer was extracted with ethyl acetate, and the combined organic layers were washed with 5 N NaOH, dried over Na$_2$SO$_4$, and evaporated under reduced pressure. The solid residue was washed with methanol, collected, and dried to afford **16** as a pale-yellow solid in 65% yield; mp (methanol) 152−155 °C. ^{1}H NMR (300 MHz, DMSO-d_6) δ 10.41 (s, 1H), 8.65 (d, J = 9.0 Hz, 1H), 8.47 (d, J = 6.6 Hz, 1H), 8.25 (s, 1H), 7.87−7.77 (m, 2H), 7.34−7.29 (m, 5H), 7.12−6.89 (m, 2H), 6.89−6.67 (m, 2H), 4.64 (s, 2H), 4.57 (s, 2H). ^{13}C NMR (75 MHz, DMSO) δ 163.1, 153.5, 152.7, 150.7, 143.2, 138.2, 138.1, 130.4, 129.2, 128.3, 127.9, 127.3, 126.7, 121.9, 118.8, 114.2, 113.9, 109.6, 102.7, 59.1, 48.1. MS (ESI) m/z 415 [M + H]$^+$.

4-(Pyrrolidin-1-ylmethyl)benzonitrile (18). To a mixture of **17** (1.00 g, 7.63 mmol), pyrrolidine (630 μL, 7.63 mmol), and acetic acid (300 μL), pic-BH$_3$ (0.816 g, 7.63 mmol) was added over 5 min and the reaction mixture was stirred at 25 °C for 3 h. Thereafter, 10% acetic acid was added and the solution was stirred at 25 °C for 30 min. A saturated solution of Na$_2$CO$_3$ was added, the aqueous layer was extracted with ethyl acetate, and the combined organic layers were washed with brine, dried over Na$_2$SO$_4$, and evaporated under reduced pressure. The crude product was purified by silica gel flash chromatography (10% water in acetonitrile) to afford **18** as a pale-yellow oil in 60% yield. ^{1}H NMR (300 MHz, CDCl$_3$) δ 7.59 (d, J = 8.2 Hz, 2H), 7.45 (d, J = 8.2 Hz, 2H), 3.66 (s, 2H), 2.61−2.40 (m, 4H), 1.86−1.73 (m, 4H). MS (ESI) m/z 187 [M + H]$^+$.

N-((4-(Pyrrolidin-1-ylmethyl)phenyl)methyl)amine (19). To a solution of **18** (0.65 g, 3.50 mmol) in ethanol (15.0 mL), NiCl$_2$·6H$_2$O (0.83 g, 3.50 mmol) was added. Afterward, NaBH$_4$ (1.036 g, 28 mmol) was added very cautiously while stirring the solution vigorously. The reaction was stirred at 25 °C for 12 h and then was filtered through a pad of Celite. The solvent was evaporated, and the crude dissolved in water and extracted with chloroform. The combined extracts were dried over Na$_2$SO$_4$ and evaporated in vacuo to afford pure **19** in 86% yield as a pale-yellow oil. ^{1}H NMR (300 MHz, CDCl$_3$) δ 7.37−7.18 (m, 4H), 3.86−3.76 (m, 2H), 3.61 (s, 2H), 2.52 (s, 4H), 1.88−1.74 (m, 4H). MS (ESI) m/z 191 [M + H]$^+$.

7-Nitro-3-(4-(pyrrolidin-1-ylmethyl)benzyl)quinazolin-4(3H)-one (20). To a suspension of **11** (1.03 g, 5.65 mmol) in dry dichloromethane (20.0 mL) cooled at 0 °C, EDC (1.19 g, 6.22 mmol), HOBt (0.84, 6.22 mmol), and Et$_3$N (865 μL, 6.22 mmol) were added and the mixture was stirred at 0 °C for 1 h. Successively **19** (1.07 g, 5.65 mmol) was added and the reaction was stirred at rt for 12 h. Thereafter, the organic mixture was washed with saturated aqueous NaHCO$_3$, dried over Na$_2$SO$_4$, and evaporated to dryness. The residue was purified by silica gel flash chromatography (5% methanol in chloroform) to afford N-(4-(pyrrolidin-1-ylmethyl)benzyl)-2-amino-4-nitrobenzamide intermediate in 70% yield as yellow−orange oil. ^{1}H NMR (300 MHz, CDCl$_3$) δ 7.50−7.37 (m, 2H), 7.37−7.20 (m, 5H), 6.66 (br, 1H), 5.86 (br, 2H), 4.55 (d, J = 5.6 Hz, 2H), 3.60 (s, 2H), 2.50 (s, 4H), 1.76 (s, 4H). MS (ESI) m/z 355 [M + H]$^+$. The above compound (1.29 g, 3.64 mmol) and formic acid (1.5 mL, 38 mmol) were heated under reflux for 3 h. After cooling to 25 °C, the mixture was poured into water, and the solution was alkalinized with diluted NaOH and extracted with chloroform. The solvent was dried over Na$_2$SO$_4$ and evaporated under reduced pressure to afford pure **20** in 91% yield as pale-yellow amorphous solid. ^{1}H NMR (300 MHz, CDCl$_3$) δ 8.53 (d, J = 2.1 Hz, 1H), 8.47 (d, J = 8.8 Hz, 1H), 8.25 (dd, J = 8.8, 2.1 Hz, 1H), 8.20 (s, 1H), 7.39−7.27 (m, 4H), 5.19 (s, 2H), 3.59 (s, 2H), 2.47 (s, 4H), 1.75 (s, 4H). MS (ESI) m/z 365 [M + H]$^+$.

7-((7-Chloroquinolin-4-yl)amino)-3-(4-(pyrrolidin-1-ylmethyl)-benzyl)quinazolin-4(3H)-one (21). To a solution of **20** (100 mg, 0.27 mmol) in 75% aqueous ethanol (3.0 mL), iron (99 mg, 1.78 mmol) and CaCl$_2$ (40 mg, 0.27 mmol) were added and the reaction was heated under reflux for 2 h. After cooling to 25 °C, the mixture was

filtered through a pad of Celite and the solvent was evaporated, and the resulting residue was suspended in water and the aqueous solution extracted with ethyl acetate. The crude was purified by silica gel flash chromatography (5% methanol in chloroform), affording 7-amino-3-(4-(pyrrolidin-1-ylmethyl)benzyl)quinazolin-4(3H)-one as a pale-yellow solid in 60% yield; mp (ethyl acetate/n-hexane) 193−195 °C. ^{1}H NMR (300 MHz, CDCl$_3$) δ 8.10 (d, J = 9.1 Hz, 1H), 7.99 (s, 1H), 7.46 (d, J = 7.9 Hz, 2H), 7.34 (d, J = 7.9 Hz, 2H), 6.85−6.74 (m, 2H), 5.14 (s, 2H), 4.24 (s, 2H), 3.84 (s, 2H), 2.80 (br, 4H), 1.92 (br, 4H). MS (ESI) m/z 335 [M + H]$^+$. To a solution of the above compound (130 mg, 0.39 mmol) in ethanol (3.0 mL), 4,7-dichloroquinoline (77 mg, 0.39 mmol) and pyridinium chloride (49 mg, 0.43 mmol) were added. The reaction was heated under reflux for 18 h. Thereafter, the solvent was removed and the resulting residue treated with 1 N NaHCO$_3$ and extracted with chloroform. The crude was then purified by alumina column chromatography (chloroform), affording **21** as white solid in 78% yield; mp (n-hexane) 205−207 °C. ^{1}H NMR (300 MHz, CDCl$_3$) δ 8.70 (d, J = 5.2 Hz, 1H), 8.30 (d, J = 8.7 Hz, 1H), 8.08 (s, 2H), 7.93 (d, J = 9.0 Hz, 1H), 7.55−7.43 (m, 2H), 7.39−7.27 (m, 5H), 6.98 (s, 1H), 5.17 (s, 2H), 3.60 (s, 2H), 2.49 (br, 4H), 1.77 (br, 4H). ^{13}C NMR (75 MHz, CDCl$_3$) δ 160.6, 152.2, 150.2, 150.1, 147.6, 146.4, 145.4, 135.9, 134.5, 129.8, 129.5, 129.1, 128.2, 127.1, 121.9, 119.7, 119.6, 117.5, 115.5, 106.3, 60.4, 54.4, 49.5, 23.6. MS (ESI) m/z 496 [M + H]$^+$.

Measurements of CQ Transport in *X. laevis* Oocytes Expressing PfCRT. Expression of wild-type and CQ resistance-conferring forms of PfCRT (from the strains D10 and Dd2, respectively) at the plasma membrane of *X. laevis* oocytes was achieved as described previously.[31] Briefly, oocytes were injected with cRNA encoding PfCRT (20 ng per oocyte) and the uptake of [^{3}H]CQ (0.3 μM; 20 Ci/mmol; ARC) was measured 3−5 days postinjection as detailed elsewhere.[31] Uptake measurements were made over 1.5−2 h at 27.5 °C in medium that contained 96 mM NaCl, 2 mM KCl, 1 mM MgCl$_2$, 1.8 mM CaCl$_2$, 10 mM MES, 10 mM Tris-base (pH 6.0), and 15 μM unlabeled CQ. Statistical comparisons were made with the Student's t-test for unpaired samples or with paired ANOVA in conjunction with Tukey's multiple comparisons test.

Parasite Growth and Drug Susceptibility Assay. *P. falciparum* D10 and W2 Strains. The CQS (D10) and the CQR (W2) strains of *P. falciparum* were sustained in vitro as described by Trager and Jensen.[62] Parasites were maintained at 5% hematocrit (human type A-positive red blood cells) in RPMI 1640 (EuroClone, Celbio) medium with the addition of 1% AlbuMax (Invitrogen, Milan, Italy), 0.01% hypoxanthine, 20 mM Hepes, and 2 mM glutamine. All cultures were maintained at 37 °C in a standard gas mixture consisting of 1% O$_2$, 5% CO$_2$, and 94% N$_2$. Compounds were dissolved in DMSO and then diluted with medium to achieve the required concentrations (final DMSO concentration <1%, which is nontoxic to the parasite). Drugs were placed in 96-well flat-bottom microplates (COSTAR) and serial dilutions made. Asynchronous cultures with parasitemia of 1−1.5% and 1% final hematocrit were aliquoted into the plates and incubated for 72 h at 37 °C. Parasite growth was determined spectrophotometrically (OD$_{650}$) by measuring the activity of the parasite lactate dehydrogenase (pLDH), according to a modified version of Makler's method in control and drug-treated cultures. Antiplasmodial activity is expressed as the 50% inhibitory concentrations (IC$_{50}$), and each IC$_{50}$ value is the mean ± standard deviation of at least three separate experiments performed in duplicate.

Solubility Assay. Standard and sample solutions were prepared from a 10 mM DMSO stock solution using an automated dilution procedure. For each compound, three solutions were prepared: one to be used as standard and the other two as test solutions. Standard: 250 μM standard solution in acetonitrile/buffer, with a final DMSO content of 2.5% (v/v). Test sample for pH 3.0: 250 μM sample solution in acetic acid 50 mM, pH 3, with a final DMSO content of 2.5% (v/v). Test sample for pH 7.4: a 250 μM sample solution in ammonium acetate buffer 50 mM, pH 7.4, with a final DMSO content of 2.5% (v/v). The 250 μM product suspensions/solutions in the aqueous buffers were prepared directly in Millipore MultiScreen-96 filter plates (0.4 μm PTCE membrane) and sealed. Plates were left for

24 h at 25 °C under orbital shaking to achieve "pseudo-thermodynamic equilibrium" and to presaturate the membrane filter. Product suspensions/solutions were then filtered using centrifugation, diluted 1:2 with the same buffer solution, and analyzed by UPLC/UV/TOF-MS, using UV detection at 254 nm for quantitation. Solubility was calculated by comparing the sample and standard UV areas: $S = (A_{smp} \times FD \times C_{st})/A_{st}$, where S was the solubility of the compound (μM), A_{smp} was the UV area of the sample solution, FD was the dilution factor (2), C_{st} was the standard concentration (250 μM), and A_{st} was the UV area of the standard solution.

Metabolic Stability Assay. Compounds in 10 mM DMSO solution were added to an incubation mixture in a 96-well microplate containing 20 pmol/mL of hCYP3A4 (0.1−0.2 mg/mL protein). The mixture was split in two aliquots: one receiving a NADPH regenerating system, the other an equal amount of phosphate buffer. The final substrate concentration was 1 μM along with 0.25% of organic solvent. Incubation proceeded for 1 h at 37 °C and was stopped by addition of acetonitrile to precipitate proteins. Metabolic stability was given as the percent remaining following incubation with cofactor (NADPH) with reference to the incubation mixture without NADPH: % remaining = Area NADPH × 100/Area ctrl, where Area ctrl was the MS peak area of the sample solution without NADPH and Area NADPH was the MS area of the sample solution with NADPH. The % CV obtained was typically within 10%.

***In Vitro* Intrinsic Clearance (Human, Rat and Mouse Liver Microsomes).** Test compound (**6b**) was incubated separately at 1 μM concentration in 100 mM phosphate buffer (pH 7.4) with 0.2 mg/mL rat and mouse hepatic microsomal protein or 0.4 mg/mL for human liver microsomes. (Pooled human liver; BD Biosciences Woburn, MA, USA). The enzymatic reaction was started by addition of a NADPH regenerating system (final concentrations: 1 mM β-nicotinamide adenine dinucleotide phosphate reduced (NADPH) + 10 mM glucose-6-phosphate (G6P) + 0.4 U/mL glucose-6-phosphate dehydrogenase (G6PDH) as previously reported.[63] Reactions were stopped at regular time intervals (0−45 min) by adding an equal volume of acetonitrile. All incubations were performed in duplicate. Verapamil as positive control for the assay was incubated in parallel under the same conditions. Samples were analyzed by HPLC-MS. Quantitative data were automatically produced using the OpenLynx software. Calculations Substrate depletion data (peak area at different time points) were fitted to a monoexponential decay model under the assumption that the concentration of 1 μM was far below the K_m of the test compound, the intrinsic clearance (Cl$_{int}$) was calculated by eq 1

$$Cl_{int} = k(min - 1) \times [V]/[P] \qquad (1)$$

where k is the rate costant for the depletion of substrate, V is the volume of incubation in μL, and P is the amount of microsomal proteins in the incubation in mg according to Baranczewski et al.[64]

Compounds were defined as low, medium, or highly metabolized based on the in vitro CL$_{int}$ values: < 3.4 low, 3.4−92.4 medium, > 92.4 high.

Toxicity Evaluation. *Materials*. Dulbecco's Modified Eagle's Medium (DMEM) and Eagle's Minimum Essential Medium (EMEM), trypsin solution, and all the solvents used for cell culture were purchased from Lonza (Switzerland). Mouse immortalized fibroblasts NIH3T3 were purchased from American Type Culture Collection (USA) and human caucasian hepatocyte carcinoma cells HepG2 from The European Collection of Cell Cultures (UK). The mutagenicity assay was supplied by Biologik srl (Trieste, Italy).

Cell Cultures and Cytotoxicity Assay. The NIH3T3 and HepG2 cell lines were used in the cytotoxicity experiments. NIH3T3 cells were maintained in DMEM and HepG2 cells in EMEM at 37 °C in a humidified atmosphere containing 5% CO$_2$. The culture media were supplemented with 10% fetal calf serum (FCS), 1% L-glutamine−penicillin−streptomycin solution, and 1% MEM Non-Essential Amino Acid Solution. Once at confluence, cells were washed with PBS 0.1 M, taken up with trypsin−EDTA solution, and then centrifuged at 1000 rpm for 5 min. The pellet was resuspended in medium solution (dilution 1:15). Cell viability after 24 h of incubation with the different compounds was evaluated by Neutral Red Uptake (Sigma-Aldrich,

Switzerland) by the procedure previously reported.[65] The data processing included the Student's t test with $p < 0.05$ taken as significance level.

Mutagenicity Assay: Ames Test. The TA100 and TA98 strains of *Salmonella typhimurium* were utilized for mutagenicity assay. Approximately 10^7 bacteria were exposed to six concentrations of each test compound in the presence or in the absence of rat liver S9 fraction, as well as a positive and a negative control, for 90 min in medium containing sufficient histidine to support approximately two cell divisions. After 90 min, the exposure cultures were diluted in pH indicator medium lacking histidine and aliquoted into 48 wells of a 384-well plate. Within two days, cells which had undergone the reversion to *His* grew into colonies. Metabolism by the bacterial colonies reduced the pH of the medium, changing the color of that well. This color change can be detected visually or by microplate reader. The number of wells containing revertant colonies were counted for each dose and compared to a zero dose control. Each dose was tested six times.

In Vivo Antiplasmodial Activity Studies. The in vivo evaluation of therapeutic activity was performed on compounds **5a** and **6b,c** according to the standard Peters 4-day test, using the rodent malaria parasite *Plasmodium berghei* ANKA (CQ-sensitive) and, as hosts, female, 5-week-old BALB/c mice, weighing 19 ± 2 g each. For each compound, groups of each mice each were intraperitoneally inoculated with 2×10^7 *P. berghei*-infected erythrocytes. Freshly prepared aqueous stock solutions (100 mg/mL) of compounds **6b,c** were serially diluted 1.5-fold to obtain 6−7 escalating doses from 4.4 to 50 mg/kg. Each experimental group was administered daily with one dose through oral gavages of 200 μL each. Compound **5a** was administered intraperitoneally at 50 mg/kg to a single group of six mice. Treatments started 4 h after the infection and were repeated until day 4. Twenty-four hours after the last treatment, % parasitemia was counted on Giemsa smears taken from tail blood, and the mice were sacrificed by CO_2 asphyxiation. The compounds' ED_{50} mg/kg was determined by nonlinear regression (four-parameter logistic curve fit), using SigmaPlot v.10.

hERG Assay. *mRNA in Vitro Transcription.* The hERG clone was propagated in the *E. coli* strains TOP10. In vitro transcription was performed with the "mMessage mMachine" kit (Ambion, Paisley, UK) with T7 RNA polymerase using a *Eco*RI restriction enzyme recognition site for the linearization. To record macroscopic current, cRNA encoding for the channel was injected in *Xenopus laevis* oocytes (0.2 mg/mL), and K^+ currents were recorded with the patch-clamp technique 2−3 days after injection.

Oocyte Preparation and Injection. Oocytes were dissected from anesthetized *Xenopus* leavis (African clawed frogs) by surgical harvest of oocytes. Oocytes were treated with collagenase (2 mg/mL) for 1 h, rinsed with a Ca^{2+}-free OR-2 solution (NaCl 82.5 mM, KCl 2.5 mM, $MgCl_2$ 1 mM, Hepes-NaOH 5 mM, pH 7.6) and stored in SOS solution (NaCl 96 mM, KCl 2 mM, $CaCl_2$ 1.8 mM, $MgCl_2$ 1 mM, Hepes-NaOH 5 mM, pH 7.6, fresh penicillin 100 units/mL, streptomycin 100 μg/mL, gentamycin 50 μg/mL).

Electrophysiological Experiments. hERG currents were recorded from macropatches 2−3 days after injection.[66] The pipet and the bath solutions had the following composition: KOH 98 mM, $MgSO_4$ 1 mM, $CaCl_2$ 1.8 mM, HEPES 5 mM, Na-pyruvate 2.5 mM (pH 7.5 with methanesulfonic acid).[66] All drugs were prepared as 10 mM stock solutions in water and stored at −20 °C. On the day of experiments, aliquots of the stock solutions were diluted to the desired concentrations with the bath solution. Patch pipettes were pulled from glass capillary tubing (Warner G85150T-4) on a programmable Flaming/Brown type puller (Sutter P-87) and fire polished on a microforge using the resistive heat from a platinum wire. Patch pipettes were applied to the surface of freshly devitellinized oocytes to form electrical seals (>1 GΩ), allowing a voltage-clamp on patches of plasma membrane. Data were acquired using a Multiclamp 700B patch-clamp amplifier and a Digidata 1440A acquisition system with pClamp 10 software (Molecular Devices, Sunnyvale, CA). All experiments were performed at room temperature, 22−24 °C. Data analysis was carried out using Clampfit 10.2 software (Axon

Instruments, Union City, CA) and OriginPro 8.1 (OriginLab Corporation, Northampton, MA).

Na^+,K^+-ATPase assay. *Isolation of Na^+,K^+-ATPase.* Membrane fragments containing Na^+,K^+-ATPase were obtained by extraction from the outer medulla of rabbit kidneys using procedure C of Jørgensen.[67] Protein concentration was determined by the Lowry method[68] using bovine serum albumin as a standard. The total protein content of membrane fragments was usually comprised between 1.5 and 2.5 mg/mL and specific ATPase activity was in the range of 1700−2100 μmol P_i/(h·mg protein) at 37 °C.

Measurements of ATPase Activity. ATPase activity was determined by measuring production of P_i by the malachite green colorimetric method.[69] The reaction mixture included 25 mM MOPS, pH 7.0, 100 mM NaCl, 20 mM KCl, and 3 mM $MgCl_2$. Membrane fragments containing the Na^+,K^+-ATPase were added to yield approximately 1 μg/mL protein concentration. The temperature was maintained at 37 °C, and the reaction was started by addition of 1 mM ATP. Samples were then taken at serial times for P_i determination. Background activity was determined in the absence of NaCl.

Computational Details. *Preparation of Molecules.* Three-dimensional structure building was carried out on Cooler Master Centurion 5 (Intel Core2 Quad CPU Q6600 @ 2.40 GHz) with Ubuntu 10.04 LTS (long-term support) operating system running Maestro 9.2 (Schrödinger, LLC, New York, NY, 2011).[35] Molecular energy minimizations were performed in MacroModel[70] using the Optimized Potentials for Liquid Simulations-all atom (OPLS-AA) force field 2005.[71,72] The solvent effects are simulated using the analytical Generalized-Born/Surface-Area (GB/SA) model,[73] and no cutoff for nonbonded interactions was selected. Polak-Ribiere conjugate gradient (PRCG)[74] method with 5000 maximum iterations and 0.001 gradient convergence threshold was employed. The conformational searches were carried out by application of the MCMM (Monte Carlo Multiple Minimum) torsional sampling method, performing automatic setup with 21 kJ/mol (5.02 kcal/mol) in the energy window for saving structure and a 0.5 Å cutoff distance for redundant conformers. All compounds reported in this paper were treated by LigPrep application (version 2.5, Schrödinger, LLC, New York, NY, 2011), implemented in Maestro suite 2011, generating the most probable ionization state of any possible enantiomers and tautomers at vacuolar pH values (5.5 ± 0.5) for compound **3** and at cellular pH (7 ± 2) for all compounds. The intramolecular H-bonds for selected compounds were retrieved by measurements application tool implemented in Maestro graphical interface.

P450 SOM Workflow. Sites of metabolism for all molecules reported in this study were predicted by P450 site of metabolism (P450 SOM)[75] workflow implemented in Schrödinger suite 2011 (Schrödinger, LLC, New York, NY, 2011). For each molecule, P450 SOM performed a calculation of intrinsic reactivity coupled to induced fit docking (IFD)[76] for the selected isoform of cytochrome. The reactivity rules have been parametrized in P450 SOM to predict atomic reactivity profiles for promiscuous P450 enzymes that are thought to be mostly independent of structural restrictions on the binding poses. The reactivity was predicted with a linear free energy approach based on the Hammett and Taft scheme where the reactivity of a given atom is the sum of a baseline reactivity rate and a series of perturbations determined by the connectivity.[75] The induced-fit docking approach is a variation on the normal protocol.[77] The initial sampling was enhanced by generating multiple starting conformations so that a wider range of poses is found in the initial docking stage. The initial docking includes van der Waals scaling of the receptor and alanine mutation of the most flexible residues. In the Prime refinement stage, any residue with an atom within 5 Å of any ligand pose was selected for side chain prediction. The subsequent minimization included the ligand, side chains, and backbones of the flexible residues. The ligand was then redocked into each of the low-energy protein conformations, determined by a 40 kcal/mol cutoff. There was no final scoring stage because all poses were considered in determining which atoms are sufficiently accessible to the reactive heme iron. Any atom

within the cutoff distance of 5 Å from the heme iron was considered as a potential site of metabolism.[75]

In Silico ADME+T Predictions. Biosafety of developed new molecules was also explored. Properties of new compounds were studied by applying in silico tool OSIRIS property explorer (http://www.organic-chemistry.org/prog/peo/ access date 12/03/2012) released by Actelion Pharmaceutical Ltd.

Molecular Docking Studies. Homology model of hERG channel generated by Farid and co-workers[45] was obtained by Schrödinger Web site. The model was chosen because the open conformations appear suitable for drug binding. Moreover, the authors used this model of hERG channel as a docking target for binding mode prediction of well-characterized hERG blockers, including terfenadine, sertindole, ibutilide, and clofilium. Their studies yielded converging binding modes for all mentioned ligands, which added confidence to the poses obtained.

a. Protein Preparation. The three-dimensional structure of the hERG channel was imported into Schrödinger Maestro molecular modeling environment,[35] it was submitted to protein preparation wizard implemented in Maestro suite 2011 (Protein Preparation Wizard workflow 2011; http://www.schrodinger.com/supportdocs/18/16). This protocol allowed us to obtain a reasonable starting structure of protein for molecular docking calculations by a series of computational steps. In particular, we performed three steps to (1) add hydrogens, (2) optimize the orientation of hydroxyl groups, Asn, and Gln, and the protonation state of His, and (3) perform a constrained refinement with the impref utility, setting the max RMSD of 0.30. The impref utility consists of a cycles of energy minimization based on the impact molecular mechanics engine and on the OPLS_2005 force field.[71,72]

b. Molecular Docking. Molecular Docking was carried out using GOLD 5.0.1 (Genetic Optimization for Ligand Docking) software from Cambridge Crystallographic Data Center, UK, that uses the Genetic algorithm (GA)[43] running under Ubuntu 10.04 LTS OS. This method allows a partial flexibility of protein and full flexibility of ligand. For each of the 100 independent GA runs, a maximum number of 125000 GA operations were performed. The search efficiency values were set on 200% in order to increase the flexibility of the ligands docked. The active site radius of 8 Å was chosen by XYZ coordinates from the center of the terfenadine docked by IFD into hERG homology model.[45] Default cutoff values of 2.5 Å (dH-X) for hydrogen bonds and 4.0 Å for van der Waals distance were employed. When the top three solutions attained RMSD values within 1.5 Å, GA docking was terminated. The fitness function GoldScore[44] was evaluated.

Molecular Dynamics. All molecular dynamics (MD) simulations were carried out by Desmond 3.0 package[59,60] using Maestro Molecular Modeling environment as graphical interface.[35] As a first step, the complexes hERG−6b and hERG−6c derived from docking calculations (Figure 7A and B, respectively) were imported in Maestro and in the system builder step were placed into POPC membrane and solvated into an orthorhombic box filled with water, simulated by TIP3P model.[78] OPLS_2005 force field[71,72] was applied for MD calculations. Na^+ and $\overline{Cl}^-$ ions were added to provide a final salt concentration of 0.15 M in order to simulate physiological concentration of monovalent ions.[59] Constant temperature (300 K), pressure (1.01325 bar), and surface tension (4000 barÅ) were employed with NPγT (constant number of particles, pressure, surface tension, and temperature) as ensemble class. RESPA integrator[79] was used in order to integrate the equations of motion, with an inner time step of 2.0 fs for bonded interactions and nonbonded interactions within the short-range cutoff. Nose−Hoover thermostats[80] were used to keep the constant simulation temperature, and the Martyna−Tobias−Klein method[81] was applied to control the pressure. Long-range electrostatic interactions were calculated by particle-mesh Ewald method (PME).[82] The cutoff for van der Waals and short-range electrostatic interactions was set at 9.0 Å. The equilibration of the system was performed with the default protocol provided in Desmond, which consists of a series of restrained minimizations and molecular dynamics simulations utilized to slowly relax the system. Con-

sequently, one individual trajectory for each complex of 5 ns was calculated. The trajectory files were analyzed by Simulation Event Analysis and Simulation Quality Analysis implemented in the Desmond package. The same applications were used to generate all plots concerning MD simulation presented in this study. The distances between quinazoline and quinoline moieties and key residues on hERG channel were measured by taking into account the centroids of each moiety. The movies were generated by Desmond trajectory viewer and converted to appropriate size by Virtualdub application licensed under the GNU General Public License (GPL) (http://www.virtualdub.org/).

■ ASSOCIATED CONTENT

Ⓢ Supporting Information

Low energy conformers of isoquine (IQ), amodiaquine (AQ) and halofantrine, site of metabolism prediction for compound **6b,c**, Ames test performed on *S. typhimurium* TA98 strains for compounds **5c,a** and **6c,b**, Ames test performed on *S. typhimurium* TA98 and TA100 strains in the presence of the liver fraction S9 for compounds **5a**, **6b**, and **6c**, superposition between docked poses of **6b** and **6c** and their low energy confomers, superposition between initial docked structure of **6b** and after 5 ns of MD simulation, superposition between initial docked structure of **6c** and after 5 ns of MD simulation, plots derived from MD simulation, Elemental analysis. Molecular dynamics simulation movies (AVI). This material is available free of charge via the Internet at http://pubs.acs.org.

■ AUTHOR INFORMATION

Corresponding Author
*Phone: +390577234172. Fax: +390577234333. E-mail: campiani@unisi.it.

Notes
The authors declare no competing financial interest.

■ ACKNOWLEDGMENTS

■ ABBREVIATIONS USED

WHO, World Health Organization; CQ, chloroquine; CQR, chloroquine-resistant; AQ, amodiaquine; IQ, isoquine; DV, digestive vacuole; CQS, chloroquine-sensitive; pLDH, parasite lactate dehydrogenase; PfCRT, *Plasmodium falciparum* chloroquine-resistance transporter; IFD, induced-fit docking; hERG, ether-a-go-go related gene; DMEM, Dulbecco's Modified Eagle's Medium; EMEM, Eagle's Minimum Essential Meidum; FCS, fetal calf serum

■ REFERENCES

(1) *WHO World Malaria Report 2011*; World Health Organization: Geneva, 2011; http://www.who.int/malaria/world_malaria_report_2011/en/.

(2) Murray, C. J.; Rosenfeld, L. C.; Lim, S. S.; Andrews, K. G.; Foreman, K. J.; Haring, D.; Fullman, N.; Naghavi, M.; Lozano, R.; Lopez, A. D. Global malaria mortality between 1980 and 2010: a systematic analysis. *Lancet* **2012**, *379*, 413−431.

(3) Watkins, W. M.; Sixsmith, D. G.; Spencer, H. C.; Boriga, D. A.; Kariuki, D. M.; Kipingor, T.; Koech, D. K. Effectiveness of amodiaquine as treatment for chloroquine-resistant *Plasmodium falciparum* infections in Kenya. *Lancet* **1984**, *1*, 357−359.

(4) Olliaro, P.; Nevill, C.; LeBras, J.; Ringwald, P.; Mussano, P.; Garner, P.; Brasseur, P. Systematic review of amodiaquine treatment in uncomplicated malaria. *Lancet* **1996**, *348*, 1196−1201.

(5) Anvikar, A. R.; Sharma, B.; Sharma, S. K.; Ghosh, S. K.; Bhatt, R. M.; Kumar, A.; Mohanty, S. S.; Pillai, C. R.; Dash, A. P.; Valecha, N. In vitro assessment of drug resistance in *Plasmodium falciparum* in five States of India. *Indian J. Med. Res.* **2012**, *135*, 494−499.

(6) Neftel, K. A.; Woodtly, W.; Schmid, M.; Frick, P. G.; Fehr, J. Amodiaquine induced agranulocytosis and liver damage. *Br. Med. J. (Clin. Res. Ed.)* **1986**, *292*, 721−723.

(7) Hatton, C. S.; Peto, T. E.; Bunch, C.; Pasvol, G.; Russell, S. J.; Singer, C. R.; Edwards, G.; Winstanley, P. Frequency of severe neutropenia associated with amodiaquine prophylaxis against malaria. *Lancet* **1986**, *1*, 411−414.

(8) Thomas, F.; Erhart, A.; D'Alessandro, U. Can amodiaquine be used safely during pregnancy? *Lancet Infect. Dis.* **2004**, *4*, 235−239.

(9) Maggs, J. L.; Tingle, M. D.; Kitteringham, N. R.; Park, B. K. Drug−protein conjugates. XIV. Mechanisms of formation of protein-arylating intermediates from amodiaquine, a myelotoxin and hepatotoxin in man. *Biochem. Pharmacol.* **1988**, *37*, 303−311.

(10) Harrison, A. C.; Kitteringham, N. R.; Clarke, J. B.; Park, B. K. The mechanism of bioactivation and antigen formation of amodiaquine in the rat. *Biochem. Pharmacol.* **1992**, *43*, 1421−1430.

(11) Werbel, L. M.; Cook, P. D.; Elslager, E. F.; Hung, J. H.; Johnson, J. L.; Kesten, S. J.; Mcnamara, D. J.; Ortwine, D. F.; Worth, D. F. Antimalarial Drugs 0.60. Synthesis, Antimalarial Activity, and Quantitative Structure−Activity Relationships of Tebuquine and a Series of Related 5-[(7-Chloro-4-quinolinyl)amino]-3-[(alkylamino)-methyl][1,1′-biphenyl]-2-ols and *N*-omega-Oxides1,2. *J. Med. Chem.* **1986**, *29*, 924−939.

(12) O'Neill, P. M.; Willock, D. J.; Hawley, S. R.; Bray, P. G.; Storr, R. C.; Ward, S. A.; Park, B. K. Synthesis, antimalarial activity, and molecular modeling of tebuquine analogues. *J. Med. Chem.* **1997**, *40*, 437−448.

(13) O'Neill, P. M.; Harrison, A. C.; Storr, R. C.; Hawley, S. R.; Ward, S. A.; Park, B. K. The Effect of Fluorine Substitution on the Metabolism and Antimalarial Activity of Amodiaquine. *J. Med. Chem.* **1994**, *37*, 1362−1370.

(14) Raynes, K. J.; Stocks, P. A.; O'Neill, P. M.; Park, B. K.; Ward, S. A. New 4-aminoquinoline mannich base antimalarials. 1. Effect of an alkyl substituent in the 5′-position of the 4′-hydroxyanilino side chain. *J. Med. Chem.* **1999**, *42*, 2747−2751.

(15) Madrid, P. B.; Sherrill, J.; Liou, A. P.; Weisman, J. L.; Derisi, J. L.; Guy, R. K. Synthesis of ring-substituted 4-aminoquinolines and evaluation of their antimalarial activities. *Bioorg. Med. Chem. Lett.* **2005**, *15*, 1015−1018.

(16) Madrid, P. B.; Wilson, N. T.; DeRisi, J. L.; Guy, R. K. Parallel synthesis and antimalarial screening of a 4-aminoquinoline library. *J. Comb. Chem.* **2004**, *6*, 437−442.

(17) Madrid, P. B.; Liou, A. P.; DeRisi, J. L.; Guy, R. K. Incorporation of an intramolecular hydrogen-bonding motif in the side chain of 4-aminoquinolines enhances activity against drug-resistant *P. falciparum*. *J. Med. Chem.* **2006**, *49*, 4535−4543.

(18) Burckhalter, J. H.; Tendick, F. H.; et al. Aminoalkylphenols as antimalarials (heterocyclicamino)-alpha-amino-*o*-cresols; the synthesis of camoquin. *J. Am. Chem. Soc.* **1948**, *70*, 1363−1373.

(19) O'Neill, P. M.; Ward, S. A.; Berry, N. G.; Jeyadevan, J. P.; Biagini, G. A.; Asadollaly, E.; Park, B. K.; Bray, P. G. A medicinal chemistry perspective on 4-aminoquinoline antimalarial drugs. *Curr. Top. Med. Chem.* **2006**, *6*, 479−507.

(20) Biot, C.; Taramelli, D.; Forfar-Bares, I.; Maciejewski, L. A.; Boyce, M.; Nowogrocki, G.; Brocard, J. S.; Basilico, N.; Olliaro, P.; Egan, T. J. Insights into the mechanism of action of ferroquine. Relationship between physicochemical properties and antiplasmodial activity. *Mol. Pharmaceutics* **2005**, *2*, 185−193.

(21) O'Neill, P. M.; Mukhtar, A.; Stocks, P. A.; Randle, L. E.; Hindley, S.; Ward, S. A.; Storr, R. C.; Bickley, J. F.; O'Neil, I. A.; Maggs, J. L.; Hughes, R. H.; Winstanley, P. A.; Bray, P. G.; Park, B. K. Isoquine and related amodiaquine analogues: a new generation of improved 4-aminoquinoline antimalarials. *J. Med. Chem.* **2003**, *46*, 4933−4945.

(22) Lawrence, R. M.; Dennis, K. C.; O'Neill, P. M.; Hahn, D. U.; Roeder, M.; Struppe, C. Development of a Scalable Synthetic Route to GSK369796 (*N-tert*-Butyl Isoquine), a Novel 4-Aminoquinoline Antimalarial Drug. *Org. Process Res. Dev.* **2008**, *12*, 294−297.

(23) O'Neill, P. M.; Park, B. K.; Shone, A. E.; Maggs, J. L.; Roberts, P.; Stocks, P. A.; Biagini, G. A.; Bray, P. G.; Gibbons, P.; Berry, N.; Winstanley, P. A.; Mukhtar, A.; Bonar-Law, R.; Hindley, S.; Bambal, R. B.; Davis, C. B.; Bates, M.; Hart, T. K.; Gresham, S. L.; Lawrence, R. M.; Brigandi, R. A.; Gomez-delas-Heras, F. M.; Gargallo, D. V.; Ward, S. A. Candidate selection and preclinical evaluation of *N-tert*-butyl isoquine (GSK369796), an affordable and effective 4-aminoquinoline antimalarial for the 21st century. *J. Med. Chem.* **2009**, *52*, 1408−1415.

(24) Omura, Y.; Taruno, Y.; Irisa, Y.; Morimoto, M.; Saimoto, H.; Shigemasa, Y. Regioselective Mannich reaction of phenolic compounds and its application to the synthesis of new chitosan derivatives. *Tetrahedron Lett.* **2001**, *42*, 7273−7275.

(25) Zhao, H.; Fu, H.; Qiao, R. Copper-catalyzed direct amination of ortho-functionalized haloarenes with sodium azide as the amino source. *J. Org. Chem.* **2010**, *750*, 3311−3316.

(26) Biot, C.; Glorian, G.; Maciejewski, L. A.; Brocard, J. S. Synthesis and antimalarial activity in vitro and in vivo of a new ferrocene−chloroquine analogue. *J. Med. Chem.* **1997**, *40*, 3715−3718.

(27) Sato, S.; Sakamoto, T.; Miyazawa, E.; Kikugawa, Y. One-pot reductive amination of aldehydes and ketones with alpha-picoline-borane in methanol, in water, and in neat conditions. *Tetrahedron* **2004**, *60*, 7899−7906.

(28) Khurana, J. M.; Kukreja, G. Rapid reduction of nitriles to primary amines with nickel boride at ambient temperature. *Synth. Commun.* **2002**, *32*, 1265−1269.

(29) Gemma, S.; Kunjir, S.; Coccone, S. S.; Brindisi, M.; Moretti, V.; Brogi, S.; Novellino, E.; Basilico, N.; Parapini, S.; Taramelli, D.; Campiani, G.; Butini, S. Synthesis and antiplasmodial activity of bicyclic dioxanes as simplified dihydroplakortin analogues. *J. Med. Chem.* **2011**, *54*, 5949−5953.

(30) Summers, R. L.; Martin, R. E. Functional characteristics of the malaria parasite's "chloroquine resistance transporter": implications for chemotherapy. *Virulence* **2010**, *1*, 304−308.

(31) Martin, R. E.; Marchetti, R. V.; Cowan, A. I.; Howitt, S. M.; Broer, S.; Kirk, K. Chloroquine transport via the malaria parasite's chloroquine resistance transporter. *Science* **2009**, *325*, 1680−1682.

(32) Martin, R. E.; Butterworth, A. S.; Gardiner, D. L.; Kirk, K.; McCarthy, J. S.; Skinner-Adams, T. S. Saquinavir inhibits the malaria parasite's chloroquine resistance transporter. *Antimicrob. Agents Chemother.* **2012**, *56*, 2283−2289.

(33) Dive, D.; Biot, C. Ferrocene conjugates of chloroquine and other antimalarials: the development of ferroquine, a new antimalarial. *ChemMedChem* **2008**, *3*, 383−391.

(34) *P450. Site of Metabolism Prediction*, version 1.1; Schrödinger, LLC: New York, 2011.

(35) *Maestro*, version 9.2; Schrödinger, LLC: New York, 2011.

(36) Gartiser, S.; Hafner, C.; Kronenberger-Schafer, K.; Happel, O.; Trautwein, C.; Kummerer, K. Approach for detecting mutagenicity of biodegraded and ozonated pharmaceuticals, metabolites and trans-formation products from a drinking water perspective. *Environ. Sci. Pollut. Res. Int.* **2012**, *19*, 3597−3609.

(37) Nunes, L. G.; Gontijo, D. C.; Souza, C. J.; Fietto, L. G.; Carvalho, A. F.; Leite, J. P. The mutagenic, DNA-damaging and antioxidative properties of bark and leaf extracts from *Coutarea hexandra* (Jacq.) K. Schum. *Environ. Toxicol. Pharmacol.* **2012**, *33*, 297−303.

(38) Peters, W. Drug resistance in *Plasmodium berghei* Vincke and Lips, 1948. I. Chloroquine resistance. *Exp. Parasitol.* **1965**, *17*, 80−89.

(39) Bhattacharyya, D.; Sen, P. C. The effect of binding of chlorpromazine and chloroquine to ion transporting ATPases. *Mol. Cell. Biochem.* **1999**, *198*, 179−185.

(40) Mazumder, B.; Mukherjee, S.; NagDas, S. K.; Sen, P. C. The interaction of chloroquine with transport ATPase and acetylcholine esterase in microsomal membranes of rat in vitro and in vivo. *Biochem. Int.* **1988**, *16*, 35−44.

(41) Kongsamut, S.; Kang, J.; Chen, X. L.; Roehr, J.; Rampe, D. A comparison of the receptor binding and HERG channel affinities for a series of antipsychotic drugs. *Eur. J. Pharmacol.* **2002**, *450*, 37−41.

(42) Kaplan, J. H. Biochemistry of Na,K-ATPase. *Annu. Rev. Biochem.* **2002**, *71*, 511−535.

(43) Jones, G.; Willett, P.; Glen, R. C. Molecular recognition of receptor sites using a genetic algorithm with a description of desolvation. *J. Mol. Biol.* **1995**, *245*, 43−53.

(44) Jones, G.; Willett, P.; Glen, R. C.; Leach, A. R.; Taylor, R. Development and validation of a genetic algorithm for flexible docking. *J. Mol. Biol.* **1997**, *267*, 727−748.

(45) Farid, R.; Day, T.; Friesner, R. A.; Pearlstein, R. A. New insights about HERG blockade obtained from protein modeling, potential energy mapping, and docking studies. *Bioorg. Med. Chem.* **2006**, *14*, 3160−3173.

(46) *Induced Fit: A novel method for fast and accurate prediction of ligand induced conformational changes in receptor active sites* ; Schrödinger, LLC: New York, 2006; www.schrodinger.com/productpage/14/6/75/.

(47) Boukharta, L.; Keranen, H.; Stary-Weinzinger, A.; Wallin, G.; de Groot, B. L.; Aqvist, J. Computer simulations of structure−activity relationships for HERG channel blockers. *Biochemistry* **2011**, *50*, 6146−6156.

(48) Du-Cuny, L.; Chen, L.; Zhang, S. A critical assessment of combined ligand- and structure-based approaches to HERG channel blocker modeling. *J. Chem. Inf. Model.* **2011**, *51*, 2948−2960.

(49) Durdagi, S.; Duff, H. J.; Noskov, S. Y. Combined receptor and ligand-based approach to the universal pharmacophore model development for studies of drug blockade to the hERG1 pore domain. *J. Chem. Inf. Model.* **2011**, *51*, 463−474.

(50) Imai, Y. N.; Ryu, S.; Oiki, S. Docking model of drug binding to the human ether-a-go-go potassium channel guided by tandem dimer mutant patch-clamp data: a synergic approach. *J. Med. Chem.* **2009**, *52*, 1630−1638.

(51) Lees-Miller, J. P.; Subbotina, J. O.; Guo, J.; Yarov-Yarovoy, V.; Noskov, S. Y.; Duff, H. J. Interactions of H562 in the S5 helix with T618 and S621 in the pore helix are important determinants of hERG1 potassium channel structure and function. *Biophys. J.* **2009**, *96*, 3600−3610.

(52) Masetti, M.; Cavalli, A.; Recanatini, M. Modeling the hERG potassium channel in a phospholipid bilayer: molecular dynamics and drug docking studies. *J. Comput. Chem.* **2008**, *29*, 795−808.

(53) Mitcheson, J. S.; Chen, J.; Lin, M.; Culberson, C.; Sanguinetti, M. C. A structural basis for drug-induced long QT syndrome. *Proc. Natl. Acad. Sci. U. S. A.* **2000**, *97*, 12329−12333.

(54) Pearlstein, R. A.; Vaz, R. J.; Kang, J.; Chen, X. L.; Preobrazhenskaya, M.; Shchekotikhin, A. E.; Korolev, A. M.; Lysenkova, L. N.; Miroshnikova, O. V.; Hendrix, J.; Rampe, D. Characterization of HERG potassium channel inhibition using CoMSiA 3D QSAR and homology modeling approaches. *Bioorg. Med. Chem. Lett.* **2003**, *13*, 1829−1835.

(55) Recanatini, M.; Cavalli, A.; Masetti, M. Modeling HERG and its interactions with drugs: recent advances in light of current potassium channel simulations. *ChemMedChem* **2008**, *3*, 523−535.

(56) Sintra Grilo, L.; Carrupt, P. A.; Abriel, H.; Daina, A. Block of the hERG channel by bupivacaine: electrophysiological and modeling insights towards stereochemical optimization. *Eur. J. Med. Chem.* **2011**, *46*, 3486−3498.

(57) Sanchez-Chapula, J. A.; Navarro-Polanco, R. A.; Culberson, C.; Chen, J.; Sanguinetti, M. C. Molecular determinants of voltage-dependent human ether-a-go-go related gene (HERG) K$^+$ channel block. *J. Biol. Chem.* **2002**, *277*, 23587−23595.

(58) *The PyMOL Molecular Graphics System*, version 1.5.0.1; Schrodinger LLC: New York, 2012.

(59) *Desmond Molecular Dynamics System*, version 3.0; D. E. Shaw Research, New York, 2011; *Maestro-Desmond Interoperability Tools* , version 3.0; Schrodinger LLC: New York, 2011.

(60) Bowers, K. J.; Chow, E.; Xu, H.; Dror, R. O.; Eastwood, M. P.; Gregersen, B. A.; Klepeis, J. L.; Kolossvary, I.; Moraes, M. A.; Sacerdoti, F. D.; Salmon, J. K.; Shan, Y.; Shaw, D. E. Scalable algorithms for molecular dynamics simulations on commodity clusters. In SC '06: Proceedings of the 2006 ACM/IEEE Conference on Supercomputing, Tampa, FL, November 11-17, 2006.

(61) Garg, V.; Stary-Weinzinger, A.; Sachse, F.; Sanguinetti, M. C. Molecular determinants for activation of human ether-a-go-go-related gene 1 potassium channels by 3-nitro-*N*-(4-phenoxyphenyl) benzamide. *Mol. Pharmacol.* **2011**, *80*, 630−637.

(62) Trager, W.; Jensen, J. B. Human malaria parasites in continuous culture. *Science* **1976**, *193*, 673−675.

(63) D'Elia, P.; De Matteis, F.; Dragoni, S.; Shah, A.; Sgaragli, G.; Valoti, M. DP7, a novel dihydropyridine multidrug resistance reverter, shows only weak inhibitory activity on human CYP3A enzyme(s). *Eur. J. Pharmacol.* **2009**, *614*, 7−13.

(64) Baranczewski, P.; Stanczak, A.; Sundberg, K.; Svensson, R.; Wallin, A.; Jansson, J.; Garberg, P.; Postlind, H. Introduction to in vitro estimation of metabolic stability and drug interactions of new chemical entities in drug discovery and development. *Pharmacol. Rep.* **2006**, *58*, 453−472.

(65) Rossi, C.; Foletti, A.; Magnani, A.; Lamponi, S. New perspectives in cell communication: bioelectromagnetic interactions. *Semin. Cancer Biol.* **2011**, *21*, 207−214.

(66) Jiang, M.; Dun, W.; Fan, J. S.; Tseng, G. N. Use-dependent "agonist" effect of azimilide on the HERG channel. *J. Pharmacol. Exp. Ther.* **1999**, *291*, 1324−1336.

(67) Jorgensen, P. L. Isolation of (Na$^+$ plus K$^+$)-ATPase. *Methods Enzymol.* **1974**, *32*, 277−290.

(68) Lowry, O. H.; Rosebrough, N. J.; Farr, A. L.; Randall, R. J. Protein measurement with the Folin phenol reagent. *J. Biol. Chem.* **1951**, *193*, 265−275.

(69) Lanzetta, P. A.; Alvarez, L. J.; Reinach, P. S.; Candia, O. A. An improved assay for nanomole amounts of inorganic phosphate. *Anal. Biochem.* **1979**, *100*, 95−97.

(70) *MacroModel*, version 9.9; Schrödinger, LLC, New York, 2011.

(71) Jorgensen, W. L.; Maxwell, D. S.; TiradoRives, J. Development and testing of the OPLS all atom force field on conformational energetics and properties of organic liquids. *J. Am. Chem. Soc.* **1996**, *118*, 11225−11236.

(72) Kaminski, G. A.; Friesner, R. A.; Tirado-Rives, J.; Jorgensen, W. L. Evaluation and reparametrization of the OPLS-AA force field for proteins via comparison with accurate quantum chemical calculations on peptides. *J. Phys. Chem. B* **2001**, *105*, 6474−6487.

(73) Still, W. C.; Tempczyk, A.; Hawley, R. C.; Hendrickson, T. Semianalytical Treatment of Solvation for Molecular Mechanics and Dynamics. *J. Am. Chem. Soc.* **1990**, *112*, 6127−6129.

(74) Polak, E.; Ribiere, G. Note sur la convergence de directions conjuguées. *Rev. Fr. Inform. Rech. Operation., 3e Année* **1969**, *16*, 35−37.

(75) *P450 Site of Metabolism Prediction, User Manual*, version 1.1; Schrödinger Press LLC: New York, 2011.

(76) Sherman, W.; Day, T.; Jacobson, M. P.; Friesner, R. A.; Farid, R. Novel procedure for modeling ligand/receptor induced fit effects. *J. Med. Chem.* **2006**, *49*, 534−553.

(77) *Schrödinger Suite 2011 Induced Fit Docking Protocol: Glide*, version 5.7; Schrödinger, LLC: New York, 2011; *Prime*, version 3.0; Schrödinger, LLC: New York, 2011.

(78) Jorgensen, W. L.; Chandrasekhar, J.; Madura, J. D.; Impey, R. W.; Klein, M. L. Comparison of simple potential function for simulating liquid water. *J. Chem. Phys.* **1983**, *79*, 926−935.

(79) Humphreys, D. D.; Friesner, R. A.; Berne, B. J. A Multiple-Time-Step Molecular-Dynamics Algorithm for Macromolecules. *J. Phys. Chem.* **1994**, *98*, 6885−6892.

(80) Hoover, W. G. Canonical Dynamics—Equilibrium Phase-Space Distributions. *Phys. Rev. A* **1985**, *31*, 1695−1697.

(81) Martyna, G. J.; Tobias, D. J.; Klein, M. L. Constant-Pressure Molecular-Dynamics Algorithms. *J. Chem. Phys.* **1994**, *101*, 4177−4189.

(82) Essmann, U.; Perera, L.; Berkowitz, M. L.; Darden, T.; Lee, H.; Pedersen, L. G. A Smooth Particle Mesh Ewald Method. *J. Chem. Phys.* **1995**, *103*, 8577−8593.